Millennial slip rates of the Tazang fault, the eastern termination of Kunlun fault: implications for strain partitioning in eastern Tibet

Citation	Ren, J., Xu, X., Yeats, R. S., & Zhang, S. (2013). Millennial slip rates of the Tazang fault, the eastern termination of Kunlun fault: Implications for strain partitioning in eastern Tibet. Tectonophysics, 608, 1180-1200. doi:10.1016/j.tecto.2013.06.026
DOI	10.1016/j.tecto.2013.06.026
Publisher	Elsevier
Version	Accepted Manuscript
Citable Link	http://hdl.handle.net/1957/48232
Terms of Use	http://cdss.library.oregonstate.edu/sa-termsofuse

Millennial slip rates of the Tazang fault, the eastern termination of Kunlun fault: implications for strain partitioning in eastern Tibet

Junjie Ren[1,2,3*], Xiwei Xu[2], Robert S. Yeats[3], Shimin Zhang[1]

1 Key Laboratory of Crustal Dynamics, Institute of Crustal Dynamics, China Earthquake Administration (CEA), Beijing 100085, China

2 Key Laboratory of Active Tectonics & Volcano, Institute of Geology, CEA, Beijing 100029, China

3 College of Earth, Ocean, and Atmospheric Sciences, Oregon State University, Corvallis, OR 97331, USA

*** Corresponding author:**

Junjie Ren (renjunjie@gmail.com)

Address: Institute of Crustal Dynamics, China Earthquake Administration, Xisanqi, Haidian, P. O. Box 2855, Beijing 100085, China

Phone: +86-10-62846730

Fax: +86-10-62846732

Abstract

The way of slip transformation and strain partitioning at the eastern termination of the Kunlun fault system remains unclear, and the question of whether this fault system is an important part for lateral extrusion of Tibetan crust is debatable. The Tazang fault is regarded as the easternmost continuation of the Kunlun fault system, and its late Quaternary activity is unknown. In this paper, we use displaced geomorphic features combined with radiocarbon and optically stimulated luminescence (OSL) dating to determine millennial slip rates along the Tazang fault. Our data yield a 1.4-3.2 mm/yr left-slip rate on the western Tazang fault, similar to that on the Maqu segment of the Kunlun fault. Tectonic geomorphology propose that displacement on the Kunlun fault is probably transferred to the Tazang fault via a pull-apart basin. The eastern Tazang fault has a dominant reverse motion that decreases eastward from ~1.5 mm/yr to 0.2-0.3 mm/yr at the easternmost part. Displaced terraces indicates that the eastern strand of the northern Longriba fault is active in the Holocene and has a ~0.8 mm/yr right-lateral slip rate with a ~0.3 mm/yr reverse component. Millennial slip rates and geodetic results show that the decrease of left-lateral motion along the Tazang fault is mainly transformed into crustal shortening along the nearly N-S-trending Longriba, Minjiang, and Huya faults, probably resulting in uplift of the Min Shan. Our results also indicate that the deformation along the Tazang fault is not transferred to beyond the border of the plateau, and the Kunlun fault is not an important tectonics for Tibetan extrusion.

Keywords

Tazang fault; Kunlun fault; slip rate; eastern Tibet; displaced terrace riser; Min Shan platform

1. Introduction

The collision between the Indian and Eurasian plates since the Eocene (~50 Ma) not only causes the uplift of the Tibetan Plateau and associated compressional tectonics, but also results in eastward motion of the Tibetan Plateau, and produces several large-scale intracontinental strike-slip fault systems (Fig. 1) (Molnar and Tapponnier, 1975; Tapponnier and Molnar, 1977; Harrison et al., 1992). Whether these strike-slip fault systems act on boundaries between quasi-rigid blocks or microplates (e.g. Tapponnier et al., 1982; Avouac et al., 1993; Tapponnier et al., 2001b), or whether slip along these fault systems just reflects strain localization in a continuous medium (e.g. England and Houseman, 1986; Houseman and England, 1993) remains a hot debate. In a sense, this debate has been translated into a question of whether slip rates on these strike-slip faults are rapid (e.g., Tapponnier et al., 2001a; Mériaux et al., 2005) or slow (e.g. Cowgill, 2007; Gold et al., 2011). However, although decadal geodetic data suggest distributed deformation throughout the plateau and support the latter (e.g. Zhang et al., 2004), whether GPS velocity across these major fault system is continuous or not depends on the spatial scale. Recent studies (e.g.,Gan et al., 2007; Zheng et al., 2013) indicated abrupt decrease of GPS velocity across these active faults. In addition, understanding the role of these major strike-slip faults will test the way in which continental crust deform in response to the India-Eurasia collision and eastward motion of the Tibetan Plateau.

Several active strike-slip fault systems are known to terminate in deforming regions in the Tibetan Plateau. Displacement on the Altyn Tagh and Haiyuan faults in the northern Tibet is transformed into shortening in the Qilian Shan (e.g. Burchfiel et al., 1989; Tapponnier et al., 1990) and Liupan Shan (e.g. Zheng et al., 2013), respectively. Slip on the Karakorum fault is converted into extension at its south tip (Murphy et al., 2002; Yin, 2010). Among these strike-slip faults, the Kunlun fault system is considered an important part of eastward extrusion of the Tibetan Plateau (Tapponnier and Molnar, 1977). Recent studies indicated that the eastern termination of the Kunlun fault is related to gradual eastward decrease in slip rates (Kirby et al., 2007; Harkins et al., 2010; Li et al., 2011; Kirby and Harkins, 2013). However, the eastern termination of this fault system is debatable. One view is that the Kunlun fault system was thought to terminate near the Roergai basin (~102ºE) (Fig. 1b) , and the displacement along the fault system is not transferred to other structures, but was absorbed or accommodated by internal deformation of the plateau surrounding the fault tip via regional clockwise rotation, distributed crustal thickening, or a combination (Kirby et al., 2007; Harkins et al., 2010; Kirby and Harkins, 2013). However, a recent deep seismic study (Jia et al., 2010) indicated that the Roergai basin is a more rigid subblock than neighbouring areas and includes no active structures that can accommodate the transferred deformation along the Kunlun fault system. An alternative view is that the Kunlun fault continues eastward to the Min Shan along the Bailongjiang or Tazang fault (Fig. 1a) (Chen et al., 1994; Kirby et al., 2000). A recent detailed investigation suggested an insignificant left-slip rate along the Bailongjiang fault, characterized by Quaternary folds (Eric Kirby, personal communication, 2012). Detailed investigation on the Tazang fault is lacking due to high relief. Kirby et al. (2007) proposed that the Tazang fault might be inactive since ~9 ka and accommodates a slip rate less than 1 mm/yr. This proposal appears to contradict prominent fault scarps on a late Quaternary alluvial fan and displaced streams along the Tazang fault. Moreover, the role of active structures south of the Tazang fault, such as the Longriba, Minjiang and Huya faults, in strain partitioning in eastern Tibet and their relationship with the Tazang fault remain unclear. In addition, the extrusion model predict that the Kunlun fault was generally regarded as an important tectonics to transfer deformation from central Tibet to beyond the plateau (Molnar and Tapponnier, 1975; Tapponnier and Molnar, 1977; Searle et al., 2011). The study on slip rates along the Tazang fault will evaluate this hypothesis.

Here, we map the Tazang fault based on interpretation of satellite imagery and field observations, and use displaced geomorphic features to determine its slip rate combined with topographic surveying, radiocarbon and OSL dating. In addition, we investigate the Holocene activity along the northern Longriba fault south of the Tazang fault. Finally, we explore the relationship between the master Kunlun fault system and the Tazang fault, and discuss strain partitioning at the eastern tip of the Kunlun fault. This study bears on the kinematics at the eastern termination of the Kunlun fault.

2. Geologic setting

The Kunlun fault system is one of the main components of the active deformation field in northeastern Tibet. It extends from longitude 86ºE to the eastern margin of the Plateau near the Sichuan Basin and strikes west-northwest to east-west across over 1300 km (e.g. Molnar and Tapponnier, 1975; Yin, 2010; Yeats, 2012). This fault system defines the boundary of the Bayan Har and Qaidam blocks, marking a transition from a continuous, low-relief, high-altitude plateau surface to the south to a northern domain of active fold ranges and intramontane basins (Yin and Harrison, 2000; Yin, 2010).

Significant information is available for slip rates along the Kunlun fault west of the town of Maqu (Fig. 1b). Kidd and Molnar (1988) first estimated the late Quaternary slip rate along the central segment of the fault at 10-15 mm/yr based on displaced moraines. Van der Woerd and his group determined a uniform left-slip rate of 10-12 mm/yr along the central ~600 km of the fault (Van der Woerd et al., 2000; Tapponnier et al., 2001a; Van der Woerd et al., 2002). Li et al. (2005) suggested a slip rate of ~10 mm/yr on the fault segment farther west. Such data indicate a spatially uniform slip rate along the Kunlun fault system between ~92ºE and ~100ºE (Fig. 1a). However, the slip rates determined by displaced geomorphic features and paleoseismology along the eastern part of the Kunlun fault (between ~100ºE and 102ºE) decrease from ~6-7 mm/yr to ~2-3 mm/yr (Kirby et al., 2007; Harkins and Kirby, 2008; Lin and Guo, 2008; Harkins et al., 2010; Li et al., 2011).

The Maqu fault segment is separated from the Tazang fault by ~80 km across the Roergai basin, where marshlands are dominant, and no prominent active fault trace can be identified from geomorphic features (Fig. 1b). From satellite imagery, the Tazang fault appears to continue ~100 km eastward to form a big bend, where the fault strikes west-northwest to northwest (Fig. 1). To the north of the Tazang fault, no significant active structures are recognizable in the field or by remote sensing for over 100 km (Kirby et al., 2007). The southern side of the Tazang fault is marked by the Min Shan platform (Chen et al., 1994), including nearly north-south-trending compressional structures, such as the Minjiang, Huya and Longriba faults (Fig. 1). The Min Shan platform can be divided into western and eastern parts by the Minjiang fault. The eastern part is characterized by high relief and is bounded by the Huya fault in the east (Burchfiel et al., 1995; Kirby et al., 2000), whereas the western part is expressed by relatively low relief. The western margin of the Min Shan platform appears to be bounded by the western strand of the Longriba fault (Xu et al., 2008) and is also the divide of the Yellow and Yangtse River drainage systems. To the west, streams such as the Hei and Bai rivers flow into the Yellow River; to the east, streams such as the Tala, Remo and Gaima rivers enter the Minjiang or Bailong river that finally joins the Yangtse River (Fig. 1). South of these

N-S-trending structures, the northeast-trending Longmen Shan fault zone bounds the eastern margin of the Tibetan Plateau against the Sichuan basin and is dominantly a thrust with a right component (Fig. 1a) (Burchfiel et al., 1995; Xu et al., 2009; Ren et al., 2010; Ren et al., 2012).

The central and eastern parts of the Kunlun fault system have also experienced a series of large earthquakes over the past century (Fig. 1a), including the 2001 Kokoxilli earthquake (Mw 7.8) that generated a ~450 km long surface rupture with a maximum strike-slip displacement of ~16 m along the Kusai Lake segment (Klinger et al., 2005). Along with the 1997 Mayi (Mw 7.6) (Peltzer et al., 1999), 1937 Tuosuo Lake (M 7.5) (Guo et al., 2007), and two smaller earthquakes, nearly the entire fault except the Maqu and Minshan segments has undertaken historic ruptures. A recent paleoseismic investigation on the Maqu segment revealed that this fault segment has experienced at least nine surface-faulting events over the past 9000-10000 yr (Lin and Guo, 2008). In contrast, the Tazang fault has experienced little historic seismicity (China Earthquake Administration, 1999). Moreover, other fault systems around the eastern tip of the Kunlun fault have undergone numerous earthquakes, for example, the 1933 M 7.5 and 1960 M 6.7 events on the Minjiang fault (Chen et al., 1994), the 1976 Songpan earthquake swarm including two M 7.2 shocks on the Huya fault (Jones et al., 1984), the 2008 Wenchuan Mw 7.9 earthquake on the Longmen Shan fault (Xu et al., 2009), although the record of historic earthquakes is only a few hundred years long (Huang et al., 1994). Additionally, the 1879 M ~8 earthquake was inferred possibly associated with a fault east of the Tazang fault (Liu et al., 2012). Considering the seismicity east and west of the Tazang fault, we infer that the Tazang fault might be also seismically active. Focal mechanisms indicate that the Kunlun fault is dominantly left-lateral slip, and other fault systems at the east tip of the Kunlun fault are primarily thrusting motion (Fig. 1), consistent with geodetic results (Gan et al., 2007).

Satellite image indicates that the Tazang fault extends from the northeastern margin of the Roergai basin, through the northern margin of the Min Shan platform and to east of the town of Tazang. Geometrically, it is divided into western and eastern segments separated by the Muduo constraining stepover at ~103.3 ºE (Fig. 1b). The western segment extends ~30 km along the mountain front west of the town of Axi. The fault trace is characterized by a striking linear feature and fault scarps (Fig. 2a). This segment strikes west-northwest (~280-300º), similar to the master Kunlun fault. In contrast, the eastern segment of the Tazang fault runs across high mountains and is primarily marked by linear deep-cut channels. The eastern segment turns southward from north of Qiuji town and trends northwest (~310-320º). Between Dongbei village and Tazang town, the Tazang fault appears to link with nearly north-south-striking faults (Fig. 1b).

In this study, topographic survey by Real Time Kinematic (RTK) GPS is used to determine the displacement, and radiocarbon and OSL dating are used to constrain the ages of displaced geomorphic surfaces. Lateral offset of faulted terrace riser is determined by the approach of Gold et al. (2011) that considers two projections for each riser crest on the fault to estimate minimum and maximum offsets (see Gold et al. (2011) for detailed illustration of this approach).

3. Western segment of Tazang fault

The western segment of the Tazang fault runs across the mountain front west of the Axi river (Fig. 1b). Numerous gullies (named G1-G8 in Fig. 2b) cut the mountains in the northeast and join the Axi river draining into the Roergai basin. This segment comprises two sub-segments separated by a small left-stepping pull-apart basin expressed by sag ponds (Fig. 2b). Northwest of gully G3, a frontal alluvial fan suggests relative uplift north of the fault. The fault trace is characterized by offset channels, sag ponds and northeast-facing scarps on the alluvial fan. Southeast of gully G3, the fault is marked by fault scarps, linear fault valleys, and offset interfluves and channels. On the interfluves, the fault forms an uphill-facing scarp that separates low bedrock hills to the south from high-relief topography to the north. Two terraces are developed along gullies G3-G7 (Fig. 2b). Our work focused on alluvial fan and gullies G3-G5.

3.1 offset channels on the alluvial fan

The Tazang fault cuts across the alluvial fan west of gully G3 and forms a northeast-facing scarp, resulting in sag ponds at the front of scarp. Some channels are deflected along the fault. Gully G2 cuts the alluvial fan and splays into several creeks at the fan front (Fig. 2b), suggesting that gully G2 may have developed when the alluvial fan was abandoned. Field observations indicate that no terrace forms along gully G2. Here, we use the overall trends of both channel banks to determine the minimum and maximum offsets of the gully. The gully channel north of the fault trance is narrow and straight. However, the trend of the east channel bank near the fault is not well determined because the east channel bank south of the fault trace is partially collapsed (see white areas along the gully G2 in Fig. 3a). We have to use the back edge of the collapsed parts that may yield a bigger maximum offset. Based on the above approach, the gully channel is left-laterally offset by 17-35 m (Fig. 3a). Also, a channel west of gully G2 is offset at the fault scarp. Based on the overall trends of two banks of this channel, the left-lateral offset at this site is 18-24 m. So we confidently propose that the left-lateral offset of the channels on the alluvial fan might be 17-35 m. In addition, two topographic profiles across the fault scarp yield the vertical separation of 1.8-4.8 m (Fig. 3b).

The fan fill consists primarily of alluvial gravel with sand lenses, capped by a ~40-cm-thick soil layer. At an exposure close to gully G3, a detrital charcoal sample (AX-C-15) collected from a fine sand lens ~1.5 m below the surface yielded an age of 13260±120 cal yr BP (Fig. 3c and Table 1). An OSL sample taken from a sand layer in the overlying soil resulted in an age of ~2.7 ka (Fig. 3c and Table 2). We interpret that the OSL age cannot be used to constrain the lower limit of the alluvial fan, because the sand layer is probably from a small stream after the abandonment of the alluvial fan. In addition, although fans do not grow in all directions all at once, sample AX-C-15 taken from the sediments ~1 m below the top of the alluvial deposits that should approximately represent the age of a period of accumulation before the fan abandonment. Detrital samples should be assumed a maximum age of the fan given the potential for charcoal to reside in soils prior to deposition. So the radiocarbon date likely represents the upper bound of the abandonment age of the alluvial fan.

3.2 Site of gully G3

In gully G3, terraces T1 and T2 are well preserved on the west bank and are ~2.5 and ~4 m high above the present river, respectively. The fault trace is characterized by prominent southwest-facing scarps on the T2 terrace on the west bank (Fig. 4a). Four topographic profiles across the fault scarp on the west bank yield a vertical separation of 80-150 cm (Fig. 4b). The younger terrace (T1) was not developed at the site that the fault crosses, so the lateral offset at gully G3 cannot be determined.

In addition, the T2 terrace on the west bank appears to be offset right-laterally (Fig. 2b). Field observation shows that no fault scarp and displaced T1/T2 riser were found on both banks of gully G3. A wide channel from the northern end of the T2 terrace south of the fault may have taken an important role in the formation of terrace T2 on the west bank. This channel and gully G3 might be important streams for the alluvial fan. Due to some reason, the alluvial fan was elevated and abandoned. Gully G3 began to downcut the alluvial fan and formed the present G3 and terrace T2. This wide channel eroded the alluvial fan and formed the wide terrace T2 on the west bank. Due to faulting of the Tazang fault, the upper stream of this channel was laterally displaced. The stream has no enough capacity to continue downcut. But small creeks from the stream now can be found on terrace T2 (Fig. 2b). Therefore, this false lateral motion on terrace T2 on the west bank of gully G3 is not related to faulting.

The T2 terrace fill is composed of alluvial gravel in the lower part, poorly rounded sandy gravel in the middle part probably derived from a local small stream, and the overlying gray-black soil and turf layer (Fig. 2c). Plant material collected from within the upper alluvial gravel yielded an age of 12720±160 cal yr BP, and a peat sample taken from a peat in the slope wash was dated at 4720±140 cal yr BP (Fig. 2c and Table 1), suggesting the age of the T2 terrace at 12.7-4.7 ka, broadly consistent with regional studies (Kirby et al., 2007; Li et al., 2011).

3.3 Site of gully G4

In gully G4, terraces T1 and T2 are well developed and are ~2.5 and ~4.5 m high above the present channel, respectively. The Tazang fault consists of two strands (S1 and S2) (Fig. 2b). The S1 strand is characterized by a fault valley and fault scarp (Fig. 5a). Topographic profiles across the scarp on terrace T2 yield a vertical separation of 1.5-1.8 m (Fig. 5b). On the southeast bank of gully G4, The T1/T2 riser at the fault location is obscure due to cover and erosion by a marsh, and no significant offset was found (Fig. 5a, c). We infer that the S1 strand may have a minor left-lateral motion.

The S2 strand is marked by a linear feature (Fig. 6a), showing displaced T2/T1 riser on the east bank of gully G4. Because the riser crest was dissected by small creeks, we determine the left-lateral slip of the T2/T1 riser by the intersection of the base of the riser with the lower tread. The base line of the riser is oblique to the fault trace and is partially eroded by a creek, producing a curve base line. Here, we use the trend lines near and off the fault to determine the offset range following the approach of Gold et al. (2011). Topographic survey yields a left-lateral offset of the T2/T1 riser by 16-24 m (Fig. 6c). On the west bank, the T1 terrace on the south side of the fault is not preserved (Fig. 6b,e).

In the gully channel where the S2 fault strand passes through, a fault exposure was found at the T1/floodplain riser (Fig. 7). Unit 1 is grey black soil consisting of grass roots. Unit 2 is a paleo-turf composed of decayed grass roots. The bottom of Unit 3 is the mixture of yellowish clasts and grey sand, and the top part is oriented clasts along the slope. We infer that unit 3 might represent a small colluvial wedge. Unit 4 is grey-black alluvial gravel. Unit 5 is orange fine sand. Unit 6 are grey-black sand with clasts. Unit 7 is orange sand with fine clasts. Unit 8 is yellowish sand with clasts and grey silt interbeds. Unit 9 is marsh silt with fine clasts.

The presence of the fault is based on the following evidence. First, the site of this exposure is on the strike of the linear feature (Fig. 6a). Second, there are oriented clasts between the contact of these units, whereas the clasts off the fault orients plane (Fig. 7). Third, although the contrast of the units on the two sides of the fault is not distinctive, their differences can be distinguished by detailed observations. Unit 6 is grey-black and unit 7 is orange, whereas unit 8 is yellowish with thin grey silts. The grain size of clasts in unit 8 is apparently bigger than that in units 6 and 7 (Fig. 7). This exposure indicates that the fault might displace units 4-9. In addition, the upward termination is a fissure filled with orange silt. We don’t determine whether the fissure is related to the activity of the fault.

A detrital charcoal sample collected from the alluvial sand (unit 5) resulted in a maximum abandonment age of terrace T1 at 4900±80 cal yr BP (Fig. 7 and Table 1). An organic sediment sample taken from within the top of unit 2 yielded a minimum age of 1930±60 cal yr BP for terrace T1 (Fig. 7 and Table 1). From this exposure,we infer that the fault was active at ~4.9 ka.

The fill of terrace T2 is composed of a lower 4 m of fine-grained alluvial sand with gravel; bedding is relatively planar (Fig. 6d). A peat ~20 cm thick covers the alluvium. The peat layer consists of grey-black clay including charcoals that should represent a paleo-surface after the abandonment of the alluvium. The age of the peat may be very close to the abandonment of the alluvium. A turf layer mantles the peat layer and includes modern grass roots in the upper part and decayed grass roots related to marsh in the lower part. Two radiocarbon samples from the terrace fill constrain the age of abandonment of terrace T2. A charcoal sample from the top of an alluvial sand yielded an age of 9150±140 cal yr BP, and another charcoal sample from the central part of the peat layer was dated at 8000±80 cal yr BP (Fig. 6d and Table 1). Kirby et al. (2007) also collected two samples from the T2 terrace fill in this gully. A peat layer in the overlying soil yielded an age of 4685±151 cal yr BP, and a charcoal sample collected from the middle alluvium resulted in an age of 9132±131 cal yr BP (Kirby et al., 2007). These dates are consistent with our dating results. Based on all the dates in this gully, terrace T2 was abandoned between 9.13 and 8 ka.

3.4 Site of gully G5

On the two sides of gully G5, the fault is characterized by ~100 m wide fault valley occupied by marsh (Fig. 2b). Terraces T1 and T2 are well preserved on the west bank and are ~3.5 and ~4.5 m high above the present channel, respectively. Unfortunately, some portions of the T2/T1 riser was eroded and covered by the marsh that obscures the location of the riser (Fig. 8a). The site of offset riser was also eroded by a small creek and covered by marsh resulting in a false topography on the offset riser. This adds more uncertainties into the determination of the offset of the riser. Here, we use the trend of determined riser to measure the offset, similar to the approach of Gold et al. (2011). The near-fault riser north of the fault can be determined by control points. Following the trend of the determined riser south of the fault, we can obtain a maximum offset of 21 m. Using the trend of the inferred riser covered by marsh south of the fault, we can get a minimum offset of 15m (Fig. 8b). So the T2/T1riser in gully G5 yields a left-lateral offset of 15-21 m (Fig. 8b). No prominent scarp forms on the T1 and T2 terrace (Fig. 8b), suggesting a minor reverse component. In addition, on the east bank, terrace T2 is dominated by the marsh, and terrace T1 is not well preserved at the site where the fault passes through. So we cannot measure the offset on the east bank.

At the T1/floodplain (T0) riser, a fault exposure was found after a single excavation (Fig. 8d). This exposure includes 6 units (Fig. 9). Unit 6 in the bottom is alluvial gravel from gully G5. This unit is covered by a peat layer with fine gravel (unit 5). Unit 5 was overlain by unit 4 composed of alluvial sand and gravel with sandy silit interbeds. Unit 3 consists of decayed grass roots representing a paleo-turf. Unit 2 is alluvial sand and gravel with detrital charcoal and organic sediments. The top layer (unit 1) is the present soil with a large amount of grass roots. The fault is determined from the following evidence: (1) fault contract of several units including sub-units 2-1 (fine sand) and 2-2 (gravel), and sub-units 5-1 (black-gray) and 5-2 (gray); (2) the deformation of some units, for example, unit 3 (paleo-turf layer), unit 5 (peat layer), and several sub-layers in sub-unit 4-1; (3) oriented clasts between sub-units 4-1 and 4-2 (Fig. 9). The fault displaces alluvium and reaches the bottom of the overlying soil layer (unit 1). We infer that the two sub-units on the two sides of the fault might be contemporaneous different facies. A charcoal sample (AX-C-2) from the middle part of the alluvial sand yielded a calibrated age of 6260±60 cal yr BP. Another charcoal sample (AX-C-4) from the top alluvial sand yielded an age of 370±100 cal yr BP (Fig. 9 and Table 1). The latter charcoal may be derived from plants after the formation of the terrace and does not represent the lower limit of the T1 age, whereas the former charcoal from alluvium should be its upper limit.

Deposits of terrace T2 are composed of fine-grained alluvial silt and sand with gravel (Fig. 8c), similar to the T2 terrace in gully G4 (Fig. 6d). The alluvium is overlain by a 1.5-m-thick soil composed of turf and peat. A radiocarbon sample from the lower part of the overlying soil yielded an age of 4850±60 cal yr BP (Fig. 8c and Table 1), while a charcoal date (AX-C-10) from the top of alluvium did not contain enough ^{14}C for age analysis (Fig. 8c and Table 1). The above dates suggest that the abandonment of terrace T2 occurred prior to 4.9 ka.

3.5 Slip rates of the western Tazang fault

In the estimation of lateral slip rates using displaced riser between the upper and lower terrace, it remains debatable that the age of which terrace can be assigned to the offset riser (e.g. Cowgill, 2007; Zhang et al., 2007). On the plateau surface, gullies finally drain into the Roergai basin (Fig. 1b). These gullies generally have a small capacity of erosion. Our recent studies on the gullies along the Longriba fault zone (Ren et al., 2013a; Ren et al., 2013b) proposed the age of the upper terrace for the offset riser, consistent with the model for settings where the stream has insufficient lateral erosion capabilities to remove lateral riser offset (Lensen, 1968; Mériaux et al., 2005; Mason et al., 2006; Cowgill, 2007). Considering that the streams at the western segment of the Tazang fault have limited flux, the age of the upper terrace is used to determine strike-slip rates along the western Tazang fault.

In addition, because gullies G3-G5 share the common erosion base level (riverbed of the Axi river), they should have experienced similar amounts of aggradation and downcut. The height of their terraces above the present channel should be about the same, consistent with our observations in which the T1 and T2 terraces are ~3 and 4-5 m above the present river, respectively. Thus their terraces should have been abandoned simultaneously. In gully G3, radiocarbon dating yielded a T2 age of 4720-12720 cal yr BP. In gully G4, the dating results constrain the age of T2 of 8000-9132 cal yr BP. In gully G5, our dating suggests the abandonment of terrace T2 prior to 4.8 ka. These age data demonstrate that terrace T2 formed at 8000-9132 cal yr BP. For terrace T1, the dating results in gullies G4 and G5 yield a maximum age of ~4900 cal yr BP.

It is difficult to properly estimate the uncertainty in the calculation of slip rate from the uncertainties of age and displacement determination. Zechar and Frankel (2009) proposed a probabilistic approach that emphasizes treating age and offset estimates in terms of probability distributions and computes the slip rate distribution by convolution. Here, we employ this approach and the corresponding Matlab code (Zechar and Frankel, 2009) by Gaussian distribution to propagate the 95.4% uncertainties in the offsets and ages into calculated slip rates. On the alluvial fan, dividing the 17-35 m left-lateral offset by the maximum age of ~13 ka yields a minimum strike-slip rate of 0.8-3.4 mm/yr, and the 1.8-4.8 m high scarp produces a vertical rate of 0.1-0.3 mm/yr. East of the alluvial fan, the 16-24 m and 15-21 m offsets of T2/T1 riser yield a mean horizontal displacement of 18.9 +8.0/-6.8 m. Combined with the abandonment age of terrace T2 of 8000-9132 cal yr BP, we obtain a left-lateral slip rate of 1.4-3.2 mm/yr since ~9 ka. The measurements of fault scarps on terrace T2 yield a mean vertical separation of 1.4 +0.4/-0.5 m, indicative of a vertical slip rate of 0.1-0.3 mm/yr. These data demonstrate that the western segment of the Tazang fault is dominantly left-lateral motion.

4. Eastern segment of Tazang fault

The eastern segment of the Tazang fault extends through mountainous terrain and is characterized primarily by linear fault valleys (Fig. 1b). Some rivers originating from south of the Tazang fault such as the Tala river at Qiuji town and the Remo river at Dongbei village flow across the fault that provide insight for the late Quaternary activity of the eastern Tazang fault.

4.1. Site of Ran'an Village

North of Qiuji town, the Tala river flows northward and joins the Bailongjiang river (Fig. 1b). The fault extends from a valley west of Ran'an village across the Tala river. Fluvial terraces at the fault crossing are strongly modified by road and building construction. East of Ran'an village, a gully flows into the Tala river, and two alluvial fans develop at the merging site of streams and are named P1- P2 from younger to older (Fig. 10a, b). A south-facing scarp striking ~290-295º on the P2 fan is evidence for Quaternary activity of the Tazang fault (Fig. 10d). The bedrock ridge west of Ran'an village is not apparently laterally displaced, indicating little or no lateral slip at this site.

Two topographic profiles across the fault scarp on the P2 fan yield a vertical separation of 3.5-4.1 m

(Fig. 10b, c). To time the abandonment of the P2 fan, radiocarbon dates from two natural exposures were studied in detail. Note that all the radiocarbon dates are detrital charcoal samples. One is located at the riser of fault scarps where alluvial sediments of the middle P2 fan are well exposed. The alluvial fan is composed of alluvial gravel and an overlying soil 50 cm thick (Fig. 11a). A charcoal sample (QJ-C-5) collected from the alluvial unit, ~20 cm below the interface of soil and alluvium, yielded a calibrated age of 4460±80 cal yr BP (Fig. 11 and Table 1). Another charcoal sample (QJ-C-4) extracted from the bottom of the soil resulted in an age of 1970±80 cal yr BP (Fig. 11 and Table 1). This exposure suggests an age range of 4460-1970 cal yr BP for the abandonment of the P2 fan.

Another exposure is located near the fan front (Fig. 10b). The alluvial fan front consists of alluvial gravel in the lower part, slope wash in the middle part, and an overlying soil including large amounts of plant roots (Fig. 11b). A charcoal sample (QJ-C-2) gathered from the top of alluvial gravel yielded an age of 3060±120 cal yr BP (Fig. 11b and Table 1). Two charcoal samples were collected from within the slope wash. One sample (QJ-C-3) from its lower part was dated at 1770±80 cal yr BP, and the other charcoal sample (QJ-C-1) from its upper part yields an age of 100±140 cal yr BP (Fig. 11b and Table 1). We conclude that the latter charcoal sample may be from recent plant roots. Excluding this date, this exposure yields an age range of 3060-1770 cal yr BP for the P2 fan.

Our dating results for these two exposures constrain the abandonment age of the P2 fan between 3060 and 1970 cal yr BP. Given the vertical displacement of 3.8±0.3 m on the P2 fan, we use the approach of Zechar and Frankel (2009) to obtain the dip-slip rate of 1.5 +1.2/-0.5 mm/yr.

4.2. Site of Gouwa Village

Approximately 7 km northeast of Qiuji town, the Tazang fault extends along a tributary of Tala river (Fig. 1b). At Gouwa village, the fault is characterized by a scarp on the T2 terrace where two streams merge (Fig. 12a). Topographic profile indicates that the fault scarp is ~1.5±0.3 m high (Fig. 12a). A natural exposure shows the fault is marked by displaced alluvial gravel showing a reverse motion along the fault plane (Fig. 12b). We cannot trace the top termination of the fault due to the cover of dense plants, while the fault reaches roughly to the scarp, suggesting that the activity of this fault produced the scarp of terrace T2.

On the road to Gouwa village shown in Fig. 15b, an exposure shows that the T2 terrace fill is composed of alluvial gravel and an overlying soil ~1 m thick including clasts (Fig. 12c). A charcoal sample (QJ-C-7) collected from the bottom of the overlying soil produced an age of 1010±80 cal yr BP and another charcoal sample (QJ-C-7b) extracted from the top of alluvium yielded a similar age of 1150±80 cal yr BP (Fig. 12c and Table 1). We infer that sample QJ-C-7b may be from vegetation after the abandonment of the T2 terrace. The third charcoal sample (QJ-C-8) taken from ~20 cm below sample QJ-C-7b results in an age of 8120±120 cal yr BP (Fig. 12c and Table 1). Given that the second terrace is extensively developed in the middle-earlier Holocene in the study area, our data constrain the abandonment age of terrace T2 between 8120 and 1150 cal yr BP. Therefore, dividing the 1.5±0.3 m high displacement by the T2 age yields a broad vertical slip rate of 0.3 +1.6/-0.2 mm/yr.

4.3. Site of Dongbei Village

At Dongbei village, Remo river flows northward across the Tazang fault (Fig. 1b). Two fluvial terraces (T1 and T2) are developed along the river (Fig. 13b). Dongbei village is located on the T2 terrace (Fig. 13a). On the east bank, two alluvial fans (P1 and P2) are derived from a tributary of Remo river. The Tazang fault extends from the northeast side of a gully west of the village, through Dongbei village to the northern margin of the P2 fan (Fig. 13a, b). The fault displaced the T2 terrace and produced a prominent scarp (Fig. 13e). Topographic measurement indicates a vertical separation of 2.4-3.4 m (Fig. 13c). Terrace T1 is poorly preserved and occupied by a cement road (Fig. 13d), making it difficult to identify the displacement on this terrace.

The T2 terrace fill consists of fluvial gravel in the lower part and an overlying soil including plant roots (Fig. 13d). An OSL sample collected from a sand lens within fluvial gravel ~80 cm below the interface between the fluvial deposits and the overlying soil yielded an age of 12.48±1.10 ka (Fig. 13d and Table 2). Considering the terrace ages in this region, this age can approximately represent the upper limit of the T2 age. Thus, the minimum vertical slip rate of the Tazang fault is estimated at 0.2-0.3 mm/yr. Similarly, the bedrock ridge west of Dongbei village is not laterally offset, suggesting only minor left-lateral motion at this site. Although the evidence for strike slip on the T2/T1 riser might have been removed by the construction of the cement road, the offset on this riser may be very small. These suggest that the lateral-slip component at this site is very minor.

4.4. Summary of slip rate estimates on the eastern Tazang fault

The eastern Tazang fault has dominantly southwest-vergent thrust motion probably with no or minor left-lateral component. The fault strikes west-northwest near Qiuji town and turns to northwest at Dongbei village and Tazang town. The dip-slip rate on the Tazang fault appears to decrease gradually eastward. North of Qiuji town, the fault has a slip rate on the order of ~1.0-1.5 mm/yr. At Dongbei village, it drops to 0.2-0.3 mm/yr.

5. The Northern Longriba fault

The Longriba fault was first recognized by geodetic observations by a strong shear zone (Shen et al., 2005; Gan et al., 2007). Subsequent field investigations indicated a late-Quaternary slip rate of ~5 mm/yr (Xu et al., 2008) and strong activity of large earthquakes based on trenching (Ren et al., 2013a; Ren et al., 2013b). The Longriba fault was proposed to link northward with the Tazang fault (Xu et al., 2008). Previous work focused on the central part, whereas the sense and slip rate of the northern Longriba fault is still undetermined.

Satellite imagery reveals that the northern Longriba fault consists of at least two strands (Fig. 1b). The western strand separates the Roergai basin from the Min Shan platform. It extends from east of Meewaqu Village to east of Roergai basin and is characterized by nearly north-south-trending linear valleys (Fig. 1b). In this area, streams are generally very gentle and trend nearly north-south, consistent with local tectonics. Field observations show that these streams have not undertaken significant downcut, and no terraces are developed. No obvious scarp is found where the fault crosses terrace T2 near Meewaqu village, suggesting a minor vertical motion along this strand.

The eastern strand of the northern Longriba fault, which was previously considered the western strand of the Min Jiang fault system (Chen et al., 1994; Kirby et al., 2000), extends along the valleys of Gaima and Remo rivers (Fig. 1b). At Dongbei village, the fault is characterized by a prominent west-facing scarp on the P1 and P2 fans and appears to link with the Tazang fault (Fig. 13a, b). Along the Gaima river, the fault extends on the southeast slope and is characterized by a lineation (Fig. 14). Along the Gaimalong gully, the largest tributary of the Gaima river, two alluvial terraces are well developed (Fig. 14b). The older (T2) and younger (t1) terraces are 2.5-3 and 1-1.5 m above the present river, respectively. On the south bank, the fault displaced the T2 terrace and produced a clear scarp and the offset T2/t1 riser (Fig. 14a, b). Topographical survey at this site indicates a vertical separation of 2.4±0.2 m (Fig. 14d and and 15b), and a right-lateral offset of the T2/t1 riser of 7±1 m (Figs. 14c and 15a).

The T2 terrace fill comprises alluvial gravel in the lower part, alluvial sand and gravel with a fine sand lens in the middle, and an overlying soil (Fig. 15c). An OSL sample collected from within the fine sand lens yielded an age of 9.01±0.88 ka (Fig. 15c and Table 2). Deposits of the t1 terrace consist of the lower part of alluvial gravel, the alluvial sandy clay in the middle, and the overlying soil, and the bottom of the alluvial sandy silt was dated by OSL at 1.17±0.11 ka (Fig. 15d and Table 2). We infer that these two OSL ages represent the upper limits of the ages of the two alluvial terraces, given the dating data of terraces in this study area (Li et al., 2011).

To determine the existence of the fault, a small excavation was conducted along the fault scarp on the T2 terrace (Fig. 15b). A trench, ~0.6 m wide, ~2 m long and ~1.6 m deep, is perpendicular to the strike of the fault scarp. The exposure includes four units (Fig. 16). Unit 5, the oldest unit, is alluvial gray sandy silt with gravel probably representing the marsh deposits during the aggradation of the T2 terrace. Unit 4 is grayish alluvial gravel. Unit 3 is alluvial sand and gravel including grayish-yellow alluvial gravel in the lower part (unit 3-2), and yellowish alluvial sand with gravel in the upper part (unit 3-1). Unit 2 is composed of a bottom part with colluvial clasts and the upper part of debris-flow sand and silt with clasts, and was deposited along the scarp slope and forms a wedge, probably representing a surface-faulting event. Unit 1 is gray-black soil containing a large amount of grass roots. The fault displaces Units 4 and 3, showing a reverse motion. The trench demonstrates that the Longriba fault is responsible for the scarp on terrace T2 and the offset T2/t1 riser. A charcoal sample (DB-C-2) collected from within the top of the colluvial wedge (Unit 2) resulted in an age of 6770±100 cal yr BP (Fig. 16 and Table 1). The top of the colluvial wedge is a relatively stable slope where the detrital charcoal may be from adjacent mountain fires. We propose that the charcoal age approximately represent the age of the top of the colluvial wedge. An OSL sample taken from unit 3 yielded an age of 67.70±8.64 ka (Fig. 16 and Table 2). Given terrace ages in this region, we infer that this OSL age is unreliable, partly because the luminescence signal in the alluvial sediments might not have been bleached sufficiently (Wallinga, 2002). Our dating results suggest at least one surface-rupturing event between 9 and 6.7 ka.

Considering limited flux in the Gaimalong gully, the offset of the T2/t1 riser probably represents the displacement of the northern Longriba fault at this site since the abandonment of the T2 terrace. Therefore, the northern Longriba fault is active in the Holocene. Its right-lateral and vertical slip rate is 0.8±0.2 mm/yr and 0.3+0.1/-0.0 mm/yr, respectively. Because these OSL dates represents the maximum ages of these terraces, the slip rate estimates are minimum. At this site, the lateral-slip rate is bigger than the vertical rate, because the northeast-trending fault at this site has an angle of ~55º with the nearly east-west-directed movement (Fig. 1b). According to the vector synthesis method, the eastern strand of the northern Longriba fault is estimated to accommodate a 0.7-1.0 mm/yr crustal shortening in the east-west direction given the fault dip (57º) in the trench (Fig. 16).

6. Discussion

6.1. Relationship between the Maqu segment of the Kunlun fault and Tazang fault

Our results show that the western Tazang fault has a Holocene left-lateral slip rate of 1.4-3.2 mm/yr. It needs to note that although we propose that the age of the upper terrace is close to the real age of the riser, this age is somewhat older than the real value. Thus, the real left-lateral slip rate on the western Tazang fault should be a little higher than this value. Our result is consistent with the inference of Kirby et al. (2007) that the Tazang fault has a slow Late-Quaternary rate, but the slip rate is highly than their estimated value (>1 mm/yr).

In addition, the relationship between the Maqu and Tazang faults remains unclear, because the fault trace is obscured within marshlands of the Roergai basin. Three possiblities can be applicable to this case. Firstly, the trace of the Kunlun fault projects directly along strike toward the Tazang fault, as proposed by Li et al. (2011). But the interval between the trend lines of the two faults is ~6 km wide, and there is no obvious change of the strike on the two fault traces. Secondly, the slip on the Maqu fault is transferred onto multiple minor faults, such as the Bailongjiang and Tazang faults (Fig. 2). Geologic analysis (Kirby et al., 2007) and a recent field investigations (Eric Kirby, personal communication, 2012) suggested that the Bailongjiang fault experiences a very low left-lateral displacement in the late Quaternary, suggesting that it plays a minor part in accommodating slip. Additionally, displaced terraces yielded a millennial left-slip slip rate of 2.0±0.4 mm/yr at the eastern end of the Maqu segment (Kirby et al., 2007). The equivalent millennial slip rates with the Tazang fault imply that the Kunlun fault does not splay into numerous minor faults, but the displacement is primarily transferred to the western Tazang fault.

Thirdly, a stepover model on strike-slip faults requires that the two faults have a similar strike and slip rate. For left-lateral strike-slip faults, a pull-apart basin is developed in a left-step linking zone.

It also agrees with the case in this site. Based on satellite imagery, the linking zone is apparently characterized by a fault valley with a trend similar to overall fault strike (Fig. 17). The linear bedrock ridges south of the valley suggest that the Maqu segment of the Kunlun fault probably extends eastward. In addition, the linking zone has a depositional epicenter (Hua Lake) (Fig. 17), indicative of an extensional environment. Therefore, we propose that the Maqu segment of the Kunlun fault transmits a large part of the displacement along the Tazang fault via a pull-apart basin (Fig. 17). According to the empirical relationship of stepover width and rupture displacement on strike-slip faults (e.g., Lettis et al., 2002), the pull-apart basin appears to be wide enough (~6 km) for arresting the propagation of a ~3 m coseismic slip on the Maqu fault (Lin and Guo, 2008). Thus, the pull-apart basin can be regarded as the boundary of the Maqu and Tazang segments. The Tazang fault is the easternmost segment of the Kunlun fault. But it still needs additional geophysical work, for example, high-resolution shallow seismic reflection, to confirm the structures in the pull-apart basin.

6.2. Strain partitioning and kinematics at the eastern termination of Kunlun fault

Numerous rigid block models based on GPS data have been proposed to invert the displacement rates along the Kunlun fault (e.g. Gan et al., 2007; Thatcher, 2007; He and Chéry, 2008). In these models, the Bayan Har block was generally regarded as a rigid block in which the role of other minor structures, such as the Awancang, Longriba, Minjiang, and Huya faults, and fault segmentation of the Kunlun fault were not taken into account. The displacement rates from these models have a significant difference between geologic and geodetic rates on the eastern fault segment. A recent subblock model (Cheng et al., 2012), in which the Longriba fault divides the

Bayan Har block into two subblocks as proposed by Xu et al. (2008), yielded a left-slip rate of ~0.7 mm/yr and a thrust component of ~0.6 mm/yr for the Tazang fault, approximately coincident with our results. This coincidence suggests that the eastern part of the Kunlun fault probably follows a sub-block model. A rigid block model including more subblocks based on the ongoing results of active tectonics, should be considered to address the decrease of slip rate along the eastern Kunlun fault. In fact, there is no effective difference between sub-block and continuum deformation as the number of faults increases and the block size decreases as Thatcher (2007) proposed.

Termination of a master, rapidly slipping strike-slip fault requires that deformation should be accommodated by deformation of the crust adjacent to the fault system. Such deformation might be shown as distributed deformation in the crust surrounding the fault end, or it could be undertaken by slip on minor structures adjacent to the master fault. For the eastern termination of the Kunlun fault system, left-lateral slip rates along the Maqu fault segment and western Tazang fault appear to decrease gradually following a steady trend (Fig. 18), suggesting that the left-lateral slip on the Maqu fault is transferred to the western Tazang fault. In contrast, the eastern Tazang fault may have a very minor left-slip component, but have a dominant reverse slip that gradually decreases eastward from ~1.5 mm/yr to ~0.2-0.3 mm/yr (Fig. 18). South of the Tazang fault, numerous nearly-north-south structures including the Huya, Minjiang, and Longriba faults probably linked with the Tazang fault. Our observations indicate that the eastern strand of the northern Longriba fault is active in the Holocene and has an east-west-oriented crustal shortening of 0.7-1.0 mm/yr . Large earthquakes on the Minjiang and Huya faults (Fig. 1a) demonstrate that they are active (Chen et al., 1994). Although these faults were proposed to have a small lateral-slip component (Chen et al. (1994), Kirby et al. (2000), and this study on the Longriba fault), they have undertaken primarily nearly east-west shortening based on focal mechanisms and tectonic geomorphology (Fig. 1b).

For intraplate left-lateral strike-slip faults, Storti et al. (2003) summarized four end-member types at the fault terminations: strike-slip, rotational, extensional and contractional. The strike-slip model, in which the displacement on the master fault is distributed on numerous minor strike-slip faults, is not apparently applicable to the Kunlun fault. The rotational model predicts that the deformation of the master fault is accommodated by antithetic faults. Although the evidence for orientation of lateral slip along the Minjiang and Huya faults is lacking, offset ridges suggested a left-lateral component along the Huya fault and a right-lateral component along the Minjiang fault, but smaller than the reverse motion (Chen et al., 1994). Our results indicate that the northern Longriba fault has a right-lateral component. This tectonic environment does not result in the rotation of patches between the Huya and Minjiang faults, but we cannot exclude the possibility of rotation of the patch between the Minjiang and Longriba faults, as proposed by Harkins et al. (2010) and Kirby and Harkins (2013). However, the rotation may be very minor.

The extensional and contractional hypothesis show normal-faulting and compressional structures on the one side of the master fault, respectively. South of the Tazang fault, the nearly-N-S northern Longriba, Minjiang, and Huya faults has dominant reverse slip and east-west shortening (Chen et al., 1994; Kirby et al., 2000; Li et al., 2006); the role of the structures on the northern side is very minor (Eric Kirby, personal communication, 2012). So we propose that the Tazang fault terminates within shortening structures south of the fault. This pattern is somewhat similar to the northern termination of the Altyn Tagh fault (e.g., Burchfiel et al., 1989; Tapponnier et al., 1990), and the eastern termination of the Haiyuan fault (Zheng et al., 2013).

Moreover, the decrease of the millennial left-lateral slip rate along the Tazang fault is ~1.4-3.2 mm/yr. Our results indicate that the northern Longriba fault has a Holocene east-west crustal shortening rate of >0.7-1.0 mm/yr, whereas the late-Quaternary crustal shortening rates on the Minjiang and Huya faults are not well determined due to the lack of faulted Quaternary markers. Based on the rates of differential rock uplift, the shortening rate across the Min Shan platform is inferred to bet less than 2-3 mm/yr (Kirby et al., 2000), approximately consistent with the decrease of left-lateral slip rates along the Tazang fault.

High-precision space geodesy (GPS) provides insights for the present-day block deformation. A GPS velocity transect along the Maqu and Tazang faults indicate that the left-lateral rate along the Maqu and western Tazang faults is ~3 mm/yr, whereas the eastern Tazang fault has a minor left slip (Fig. 19b). A nearly east-west transect across the Min Shan suggests shortening rate of ~3-5 mm/yr (Fig. 19d), roughly coincident with the decrease of geodetic rate along the Tazang fault (Fig. 19b).

The approximate coincidence between the deceased left-lateral rate and crustal shortening rate across the Min Shan platform from geologic and geodetic data indicate that most of the left-lateral slip along the western Tazang fault is transformed into east-west crustal shortening along the Longriba, Minjiang and Huya faults across the Min Shan platform, as proposed by Chen et al. (1994) and Kirby et al. (2000). Only a small portion is converted into south-west-vergent reverse motion along the eastern Tazang fault.

Currently, the question of whether crustal shortening across the Min Shan results in the uplift of the Min Shan remains debatable. Chen et al. (1994) proposed that the uplift of the Min Shan are probably associated with the compression at the eastern end of the Kunlun Fault, whereas Kirby et al. (2000) thought that the lack of evidence for large-magnitude Cenozoic shortening along the eastern range front of the Min Shan and the low crustal shortening rate are insufficient to result in the uplift of the Min Shan, and suggested a driving mechanism of flow and thickening in the deep crust combined with the analysis of tectonic geomorphology (Kirby and Ouimet, 2011). Our results show that the left-lateral slip along the Tazang fault is transferred into crustal shortening across the Min Shan, as inferred by Chen et al. (1994). However, our results cannot answer the question of whether the ~2-3 mm/yr crustal shortening can lead to the uplift of the Min Shan. In fact, the similar question also exists along the Longmen Shan, where no significant Cenozoic shortening along the frontal area and low geodetic shortening rate across the Longmen Shan (~3 mm/yr) are observed. But the results from coseismic surface rupture of the 2008 Wenchuan earthquake (Xu et al., 2009) and balanced geologic cross-sections (Hubbard and Shaw, 2009) indicate that crustal shortening alone is sufficient for uplift and topography of the Longmen Shan. Thus, we infer that the relatively slow crustal shortening might be responsible for uplift of the Min Shan. Further deep seismic reflection profile across the Min Shan platform is needed to address this question.

Here, from the above illustration, we propose a model to address the kinematic mechanism at the eastern termination of the Kunlun fault. The left-lateral slip along the master Kunlun fault is transferred to the western Tazang fault via a pull-apart basin. One small portion of this left-lateral slip is converted into southwest-vergent reverse motion, and most of slip is transformed into crustal shortening along the nearly-N-S-striking structures, such as the Longriba, Minjiang, and Huya fault, resulting in the uplift of the Min Shan. The structures along with the Tazang fault merged with a decollement ~30 km deep based on the deep seismic reflection results (Wang et al., 2011).

The extrusion hypothesis of the Tibetan Plateau predicts that the deformation in the central part is transferred along the Kunlun fault beyond the border of the plateau (Molnar and Tapponnier, 1975; Searle et al., 2011). Our results reveal that the easternmost termination of the Kunlun fault (Tazang fault) undergoes minor left-lateral component. Most of the left-slip deformation from central Tibet is absorbed in the plateau. In other words, the deformation on the Kunlun fault is not transferred beyond the border of the plateau, suggesting that the Kunlun fault is not regarded as an important tectonics for lateral extrusion of Tibetan crust.

7. Conclusions

1) Based on displaced geomorphic features, the Tazang fault is active in the Holocene. The western Tazang fault undergoes a dominantly left-lateral slip rate of 1.4-3.2 mm/yr, and its eastern segment has a dominantly reverse slip rate that gradually decreases eastward from ~1.5 mm/yr to 0.2-0.3 mm/yr. The eastern strand of the northern Longriba fault is active in the Holocene and has a ~0.8 mm/yr right-lateral slip rate with a ~0.3 mm/yr reverse component.

2) The displacement along the master Kunlun fault is transferred to the Tazang fault via a pull-apart basin.

3) Only a small portion of the left-lateral slip on the Tazang fault is transformed into reverse motion on the eastern Tazang fault, and another part is converted into crustal shortening along the nearly-N-S-striking structures, probably resulting in the uplift of the Min Shan.

4) The slip along the easternmost termination of the Kunlun fault is absorbed at the eastern border of the Tibetan plateau, suggesting that the Kunlun fault is not regarded as an important tectonics for lateral extrusion of Tibetan crust.

Acknowledgements

This research was supported by the National Science Foundation of China (Grant Numbers 41102134), Institute of Crustal Dynamics, China Earthquake Administration Research Fund (Grant Number ZDJ2013-23). We thank Wenjun Kang, Shao Liu, Chenxi Li for field assistance, Junxiang Zhao for OSL analyses, Andrew Meigs, John Nabelek and Jeffrey Lee for discussions.

References

Avouac, J., Philippe, Tapponnier, P., 1993. Kinematic model of active deformation in central Asia. Geophysical Research Letters 20, 895-898.

Burchfiel, B., Chen, Z., Liu, Y., Royden, L., 1995. Tectonics of the Longmen Shan and adjacent regions, central China. International Geology Review 37, 661-735.

Burchfiel, B.C., Deng, Q., Molnar, P., Royden, L., Wang, Y., Zhang, P., Zhang, W., 1989. Intracrustal detachment within zones of continental deformation. Geology 17, 748-752.

Chen, S.F., Wilson, C., Deng, Q.D., Zhao, X.L., Luo, Z.L., 1994. Active faulting and block movement associated with large earthquakes in the Min Shan and Longmen Mountains, northeastern Tibetan Plateau. Journal of Geophysical Research 99, 20-025.

Cheng, J., Xu, X., Gan, W., Ma, W., Chen, W., Zhang, Y., 2012. Block model and dynamic implication from the earthquake activities and crustal motion in the southeastern margin of Tibetan Plateau. Chinese Journal of Geophysics 55, 1198-1212.

China Earthquake Administration, 1999. Historical Strong Earthquake Catalog of China (2300 BC -1911 AD) (in Chinese). Earthquake Publishing House, Beijing. 541pp.

Cowgill, E., 2007. Impact of riser reconstructions on estimation of secular variation in rates of strike–slip faulting: Revisiting the Cherchen River site along the Altyn Tagh Fault, NW China. Earth and Planetary Science Letters 254, 239-255.

England, P., Houseman, G., 1986. Finite Strain Calculations of Continental Deformation 2. Comparison With the India-Asia Collision Zone. Journal of Geophysical Research 91, 3664-3676.

Gan, W., Zhang, P., Shen, Z.K., Niu, Z., Wang, M., Wan, Y., Zhou, D., Cheng, J., 2007. Present-day crustal motion within the Tibetan Plateau inferred from GPS measurements. Journal of Geophysical Research 112, doi:10.1029/2005JB004120.

Gold, R.D., Cowgill, E., Arrowsmith, J.R., Chen, X., Sharp, W.D., Cooper, K.M., Wang, X.-F., 2011. Faulted terrace risers place new constraints on the late Quaternary slip rate for the central Altyn Tagh fault, northwest Tibet. Geological Society of America Bulletin 123, 958-978.

Guo, J., Lin, A., Sun, G., Zheng, J., 2007. Surface Ruptures Associated with the 1937 M 7.5 Tuosuo Lake and the 1963 M 7.0 Alake Lake Earthquakes and the Paleoseismicity along the Tuosuo Lake Segment of the Kunlun Fault, Northern Tibet. Bulletin of the Seismological Society of America 97, 474-496.

Harkins, N., Kirby, E., 2008. Fluvial terrace riser degradation and determination of slip rates on strike-slip faults: An example from the Kunlun fault, China. Geophysical Research Letters 35, doi:10.1029/2007gl033073.

Harkins, N., Kirby, E., Shi, X., Wang, E., Burbank, D., Chun, F., 2010. Millennial slip rates along the eastern Kunlun fault: Implications for the dynamics of intracontinental deformation in Asia.

Lithosphere 2, 247-266.

Harrison, T.M., Copeland, P., Kidd, W., Yin, A., 1992. Raising Tibet. Science 255, 1663-1670.

He, J., Chéry, J., 2008. Slip rates of the Altyn Tagh, Kunlun and Karakorum faults (Tibet) from 3D mechanical modeling. Earth and Planetary Science Letters 274, 50-58.

Houseman, G., England, P., 1993. Crustal Thickening Versus Lateral Expulsion in the Indian-Asian Continental Collision. Journal of Geophysical Research 98, 12233-12249.

Huang, W.Q., Li, W.X., Cao, X.F., 1994. Research on completeness of earthquake data in the Chinese mainland (II)—The regional distribution of the beginning years of basically complete earthquake data. Acta Seismologica Sinica 7, 529-538.

Hubbard, J., Shaw, J.H., 2009. Uplift of the Longmen Shan and Tibetan plateau, and the 2008 Wenchuan (M = 7.9) earthquake. Nature 458, 194-197.

Jia, S., Zhang, X., Zhao, J., Wang, F., Zhang, C., Xu, Z., Pan, J., Liu, Z., Pan, S., Sun, G., 2010. Deep seismic sounding data reveal the crustal structures beneath Zoigê basin and its surrounding folded orogenic belts. Science China Earth Sciences 53, 203-212.

Jones, L.M., Han, W., Hauksson, E., Jin, A., Zhang, Y., Luo, Z., 1984. Focal Mechanisms and Aftershock Locations of the Songpan Earthquakes of August 1976 in Sichuan, China. Journal of Geophysical Research 89, 7697-7707.

Kidd, W.S.F., Molnar, P., 1988. Quaternary and active faulting observed on the 1985 Academia Sinica--Royal society geotraverse of Tibet. Philosophical Transactions of the Royal Society of London A 327, 337-363.

Kirby, E., Harkins, N., 2013. Distributed deformation around the eastern tip of the Kunlun fault. Int J Earth Sci (Geol Rundsch), 1-14.

Kirby, E., Harkins, N., Wang, E., Shi, X., Fan, C., Burbank, D., 2007. Slip rate gradients along the eastern Kunlun fault. Tectonics 26, TC2010.

Kirby, E., Ouimet, W., 2011. Tectonic geomorphology along the eastern margin of Tibet: insights into the pattern and processes of active deformation adjacent to the Sichuan Basin. Geological Society, London, Special Publications 353, 165-188.

Kirby, E., Whipple, K.X., Burchfiel, B.C., Tang, W., Berger, G., Sun, Z., Chen, Z., 2000. Neotectonics of the Min Shan, China: Implications for mechanisms driving Quaternary deformation along the eastern margin of the Tibetan Plateau. Geological Society of America Bulletin 112, 375-393.

Klinger, Y., Xu, X., Tapponnier, P., Van der Woerd, J., Lasserre, C., King, G., 2005. High-Resolution Satellite Imagery Mapping of the Surface Rupture and Slip Distribution of the Mw 7.8, 14 November 2001 Kokoxili Earthquake, Kunlun Fault, Northern Tibet, China. Bulletin of the Seismological Society of America 95, 1970-1987.

Lensen, G.J., 1968. Analysis of progressive fault displacement during downcutting at the Branch River terraces, south Island, New Zealand. Geological Society of America Bulletin 79, 545-556.

Li, C., Xu, X., Wen, X., Zheng, R., Chen, G., Yang, H., An, Y., Gao, X., 2011. Rupture segmentation and slip partitioning of the mid-eastern part of the Kunlun Fault, north Tibetan Plateau. Science China Earth Sciences 54, 1730-1745.

Li, H., Van der Woerd, J., Paul, T., Yann, K., Qi, X., Yang, J., Zhu, Y., 2005. Slip rate on the Kunlun fault at Hongshui Gou, and recurrence time of great events comparable to the 14/11/2001, Mw∼7.9 Kokoxili earthquake. Earth and Planetary Science Letters 237, 285-299.

Li, Y., Zhou, R.J., Densmore, A.L., Ellis, M.A., 2006. The Geology of the Eastern Margin of the Qinghai-Tibet Plateau. Geological Publishing House, Beijing.

Lin, A., Guo, J., 2008. Nonuniform Slip Rate and Millennial Recurrence Interval of Large Earthquakes along the Eastern Segment of the Kunlun Fault, Northern Tibet. Bulletin of the Seismological Society of America 98, 2866-2878.

Liu, B., Yuan, D., Zhang, B., Chen, W., Niu, Y., 2012. Determinaton of fault parameters and sliding behavior of the 1879 southern Wudu M 8.0 earthquake. Seismology and Gelogy 34, 415-424 (In Chinese with English abstract).

Mériaux, A.S., Tapponnier, P., Ryerson, F.J., Xu, X., King, G., Van der Woerd, J., Finkel, R.C., Haibing, L., Caffee, M.W., Xu, Z., Chen, W., 2005. The Aksay segment of the northern Altyn Tagh fault: Tectonic geomorphology, landscape evolution, and Holocene slip rate. Journal of Geophysical Research 110, doi:10.1029/2004JB003210.

Mason, D.P.M., Little, T.A., Van Dissen, R.J., 2006. Rates of active faulting during late Quaternary fluvial terrace formation at Saxton River, Awatere fault, New Zealand. Geological Society of America Bulletin 118, 1431-1446.

Molnar, P., Tapponnier, P., 1975. Cenozoic tectonics of Asia: effects of a continental collision. Science 189, 419-426.

Murphy, M., Yin, A., Kapp, P., Harrison, T., Manning, C., Ryerson, F., Lin, D., Jinghui, G., 2002. Structural evolution of the Gurla Mandhata detachment system, southwest Tibet: Implications for the eastward extent of the Karakoram fault system. Geological Society of America Bulletin 114, 428-447.

Peltzer, G., Crampé, F., King, G., 1999. Evidence of Nonlinear Elasticity of the Crust from the Mw7.6 Manyi (Tibet) Earthquake. Science 286, 272-276.

Reimer, P., Baillie, M., Bard, E., Bayliss, A., Beck, J., Blackwell, P., Bronk Ramsey, C., Buck, C., Burr, G., Edwards, R., 2009. IntCal09 and Marine09 radiocarbon age calibration curves, 0-50,000 years cal BP. Radiocarbon 51, 1111-1150.

Ren, J., Chen, G., Xu, X., Zhang, S., Mao, C., 2010. Surface rupture of the 2008 Wenchuan, China, earthquake in the Qingping stepover determined from geomorphologic surveying and excavation, and its tectonic implications. Bulletin of the Seismological Society of America 100, 2651-2659.

Ren, J., Xu, X., Sun, X., Tan, X., Li, K., Kang, W., Liu, B., 2012. Geological and geophysical evidences of late Quaternary activity of the range-front fault along the mid-segment of the Longmen Shan thrust belt. Chinese Journal of Geophysics 55, 1929-1941.

Ren, J., Xu, X., Yeats, R.S., Zhang, S., 2013a. Latest Quaternary paleoseismology and slip rates of the Longriba fault zone, eastern Tibet: Implications for fault behavior and strain partitioning. Tectonics 32, 216-238.

Ren, J., Xu, X., Yeats, R.S., Zhang, S., Ding, R., Gong, Z., 2013b. Holocene paleoearthquakes of the Maoergai fault, eastern Tibet. Tectonophysics 590, 121-135.

Searle, M.P., Elliott, J.R., Phillips, R.J., Chung, S.-L., 2011. Crustal–lithospheric structure and continental extrusion of Tibet. Journal of the Geological Society 168, 633-672.

Shen, Z.K., Lu, J., Wang, M., Burgmann, R., 2005. Contemporary crustal deformation around the southeast borderland of the Tibetan Plateau. Journal of Geophysical Research 110, doi:10.1029/2004JB003421.

Storti, F., Holdsworth, R.E., Salvini, F., 2003. Intraplate strike-slip deformation belts. Geological Society, London, Special Publications 210, 1-14.

Tapponnier, P., Meyer, B., Avouac, J.P., Peltzer, G., Gaudemer, Y., Guo, S., Xiang, H., Yin, K., Chen, Z., Cai, S., Dai, H., 1990. Active thrusting and folding in the Qilian Shan, and decoupling between upper crust and mantle in northeastern Tibet. Earth and Planetary Science Letters 97, 382-403.

Tapponnier, P., Molnar, P., 1977. Active faulting and tectonics in China. Journal of Geophysical Research 82, 2905-2930.

Tapponnier, P., Peltzer, G., Le Dain, A.Y., Armijo, R., Cobbold, P., 1982. Propagating extrusion tectonics in Asia: New insights from simple experiments with plasticine. Geology 10, 611-616.

Tapponnier, P., Ryerson, F.J., Van der Woerd, J., Mériaux, A.S., Lasserre, C., 2001a. Long-term slip rates and characteristic slip: keys to active fault behaviour and earthquake hazard. Earth and Planetary Sciences 333, 483-494.

Tapponnier, P., Xu, Z., Roger, F., Meyer, B., Arnaud, N., Wittlinger, G., Yang, J., 2001b. Oblique Stepwise Rise and Growth of the Tibet Plateau. Science 294, 1671-1677.

Taylor, M., Yin, A., 2009. Active structures of the Himalayan-Tibetan orogen and their relationships to earthquake distribution, contemporary strain field, and Cenozoic volcanism. Geosphere 5, 199-214.

Thatcher, W., 2007. Microplate model for the present-day deformation of Tibet. Journal of Geophysical Research 112, doi:10.1029/2005JB004244.

Van der Woerd, J., Ryerson, F., Tapponnier, P., Mériaux, A.S., Gaudemer, Y., Meyer, B., Finkel, R., Caffee, M., Zhao, G., Xu, Z., 2000. Uniform slip-rate along the Kunlun fault: Implications for seismic behaviour and large-scale tectonics. Geophysical Research Letters 27, 2353-2356.

Van der Woerd, J., Tapponnier, P., Ryerson, F.J., Meriaux, A.-S., Meyer, B., Gaudemer, Y., Finkel, R.C., Caffee, M.W., Guoguang, Z., Zhiqin, X., 2002. Uniform postglacial slip-rate along the central 600 km of the Kunlun Fault (Tibet), from 26Al, 10Be, and 14C dating of riser offsets, and climatic origin of the regional morphology. Geophysical Journal International 148, 356-388.

Wallinga, J., 2002. Optically stimulated luminescence dating of fluvial deposits: a review. Boreas 31, 303-322.

Wang, C., Gao, R., Yin, A., Wang, H., Zhang, Y., Guo, T., Li, Q., Li, Y., 2011. A mid-crustal strain-transfer model for continental deformation: A new perspective from high-resolution deep seismic-reflection profiling across NE Tibet. Earth and Planetary Science Letters 306, 279-288.

Xu, X., Wen, X., Yu, G., Chen, G., Klinger, Y., Hubbard, J., Shaw, J., 2009. Coseismic reverse-and oblique-slip surface faulting generated by the 2008 Mw 7.9 Wenchuan earthquake, China. Geology 37, 515-518.

Xu, X.W., Wen, X.Z., Chen, G.H., Yu, G.H., 2008. Discovery of the Longriba fault zone in eastern Bayan Har Block, China and its tectonic implication. Science China Earth Sciences 51, 1209-1223.

Yeats, R., 2012. Active Faults of the World. Cambridge University Press, Cambridge. 625pp.

Yin, A., 2010. Cenozoic tectonic evolution of Asia: A preliminary synthesis. Tectonophysics 488, 293-325.

Yin, A., Harrison, T.M., 2000. Geologic evolution of the Himalayan-Tibetan orogen. Annual Review of Earth and Planetary Sciences 28, 211-280.

Zechar, J.D., Frankel, K.L., 2009. Incorporating and reporting uncertainties in fault slip rates. Journal of Geophysical Research 114, doi:10.1029/2009JB006325.

Zhang, P., Molnar, P., Xu, X., 2007. Late Quaternary and present-day rates of slip along the Altyn Tagh Fault, northern margin of the Tibetan Plateau. Tectonics 26, doi:10.1029/2006TC002014 .

Zhang, P., Shen, Z., Wang, M., Gan, W., Bürgmann, R., Molnar, P., Wang, Q., Niu, Z., Sun, J., Wu, J., 2004. Continuous deformation of the Tibetan Plateau from global positioning system data. Geology 32, 809-812.

Zheng, W.-j., Zhang, P.-z., He, W.-g., Yuan, D.-y., Shao, Y.-x., Zheng, D.-w., Ge, W.-p., Min, W., 2013.

Transformation of displacement between strike-slip and crustal shortening in the northern margin of the Tibetan Plateau: Evidence from decadal GPS measurements and late Quaternary slip rates on faults. Tectonophysics 584, 267-280.

Figures

Fig. 1 (a) Slip rates and seismicity along the eastern Kunlun fault zone. Focal mechanisms compiled from Harvard CMT (http://www.globalcmt.org/CMTsearch.html) and Jones et al. (1984). Earthquake data from China Earthquake Networks Center (http://www.csndmc.ac.cn/newweb/data.htm). Fault data modified after Taylor and Yin (2009). Slip rates are from Li et al. (2005) (white circle),Van der Woerd et al. (2002) (white box), Eric Kirby's group (black dot) including Kirby et al., (2007), Harkins and Kirby (2008), and Harkins et al. (2010), Li et al. (2011) (red box), and Lin and Guo (2008) (value with shaded background). Index map showing major faults of the Tibetan Plateau. Directions of block motion from GPS data (Gan et al., 2007). Blocks: [1], Qaidam block; [2], Bayan Har block; [3], Qiangtang block. (b) Topographic map of the Tazang fault and its adjacent area. See location in Fig. 1a. Background is Shuttle Radar Topography Mission (SRTM, 90 m resolution) shaded relief map. Abbreviations for active faults: ATF, Altyn Tagh fault; AWCF, Awancang fault; BLF, Bailongjiang fault; HYF, Huya fault; KF, Kunlun fault; LMSF, Longmen Shan fault; LRBF, Longriba fault; MJF: Minjiang fault; RF, Red River fault; WQF, Western Qinling fault; XF, Xianshuihe fault.

Fig. 2 Offset landforms along the western segment of the Tazang fault. Google Earth image (a) and geological map (b) showing fault scarps, sag ponds, displaced terraces (T1 and T2) and bedrock interfluves. In gully G4, the Tazang fault consists of two strands (S1 and S2). See Fig. 1b for location.

Fig. 3 Slip rate determination of the Tazang fault on the alluvial fan. (a) Google Earth image showing offset streams on the alluvial fan (N33º50'09.5", E103º02'31.6"). (b) Topographic profiles across the fault scarps surveyed by RTK GPS. (c) Stratigraphy of the alluvial fan. See their locations in Fig. 2b.

Fig. 4 (a) Fault scarps on terrace T2 on the west bank of gully G3 (N33º49’44.0”, E103º05’59.0”). (b) Topographic profiles across the fault scarp surveyed by RTK GPS. See locations on Fig. 4a. (c) Photograph of deposits of the T2 terrace of gully G3. See locations in Fig. 2b.

Fig. 5 Offset landforms along the S1 strand in gully G4 (N33º49’28.6”, E103º05’07.3”). (a) Geologic interpretation of fault trace and river terraces. See location in Fig. 2b. (b) Topographic profiles across fault scarps were surveyed by RTK GPS on the T2 terrace on the west bank. See Fig. 5a for locations. (c) Photograph showing scarp on terrace T2. Red arrows indicate fault scarps. Note that no obvious offset on the T2/T1 riser showing minor lateral slip on the S1 strand.

Fig. 6 Slip rate determination along the S2 branch in gully G4. (a) Google Earth image and (b) geologic map of faulted terraces (N33º49’18.3”, E103º05’12.0”). The fault is characterized by linear feature and displaced terrace riser shown by black arrows in Fig. 6a. See location in Fig. 2b. (c) Topographic survey of offset terrace riser using RTK GPS showing that the T2/T1 riser is displaced left-laterally by 16-24 m (see location in Fig. 6b). (d) Natural outcrop of terrace T2 of gully G4. See location in Fig. 6b. Radiocarbon samples from the upper part of alluvial sediment and the overlying peat layer are used to constrain the abandonment age of terrace T2. (e) Photograph along the projection of the T2/T1 riser shown in Fig. 6c. Two people indicate the base of the T2/T1 riser on the two sides of the fault.

Fig. 7 Natural exposure of the Tazang fault in the deposits of the T1 terrace of gully G4 (N33º49’20.70”, E103º05’10.88”). See location in Fig. 6e. The fault is marked by oriented clasts and fault layers. Ages from alluvial deposit and the overlying peat and displaced layers suggest fault activity ~4.9 ka.

Fig. 8 Slip rate determination along the gully G5. (a) Geologic map of faulted terraces (N33º49’14.7”, E103º05’44.4”). See location in Fig. 2b. (b) Topographic survey of offset terraces using RTK GPS showing that the T2/T1 riser is displaced left-laterally by 15-21 m. Yellow dots represent the locations of the T2/T1 riser determined by field observations. Dash lines show the location of the inferred risers because the marsh occupies and erodes partially the riser. (c) Natural outcrop of terrace T2 in gully G5. See location in Fig. 8d. Sample AX-C-10 does not yield an age due to insufficient ^{14}C content. (d) Photograph along the projection of the T2/T1 riser shown in Fig. 8b.

Fig. 9 Natural exposure of the Tazang fault within deposits of the T1 terrace of gully G5 (N33º49’09.78”, E103º06’08.42”). See location in Fig. 8d. The fault is characterized by offset layers and oriented clasts. See text for description of detailed strata.

Fig. 10 Offset landforms at Ran’an Village, north of Qiuji Town. (a) WorldView image and (b) geologic map of displaced alluvial fan (N33º43’36.7”, E103º21’26.3”). White arrows indicate the fault trace. See location in Fig. 1b. (c) Topographic profiles across the fault scarps on the P2 alluvial fan. See locations in Fig. 10b. (d) Photograph of fault scarp on the P2 fan, marked by white arrows.

Fig. 11 Bounds of abandonment age of the P2 alluvial fan. Samples from the middle part at fault scarp (a) and the fan front (b) suggest the formation of the P2 fan between 3060 and 1970 cal yr BP. See locations in Fig.10b.

Fig. 12 Offset landforms at Gouwa Village, east of Qiuji Town (N33º41’34.2”, E103º24’50.9”). (a) WorldView image of displaced alluvial terrace. See location in Fig. 1b. Topographic profile k-k’ (right) across the fault scarp on the T2 terrace. (b) Photograph of fault exposure in the alluvial deposit of the T2 terrace. See location in Fig. 12a. (c) The abandonment age of the T2 terrace constrained by radiocarbon samples from alluvial deposits and the overlying soil.

Fig. 13 Offset landforms at Dongbei Village (N33º28’18.1”, E103º39’51.3”). (a) WorldView image and (b) geologic map of displaced terrace and alluvial fan. Red arrows indicate the location of the fault. The bedrock ridge northwest of Dongbei Village is apparently not laterally displaced, indicating no or minor lateral slip at this site. See locations in Fig. 1b. (c) Topographic profile across the fault scarp on the T2 terrace. See location in Fig. 13b. (d) OSL sample from a sand lens in the fluvial deposits ~1m below the surface of terrace T2. See location in Fig. 13b. (e) Photograph showing displaced terrace T2 at Dongbei village.

Fig. 14 Slip rate determination of the northern Longriba fault around Gailongmalong gully. (a) Oblique satellite image from Google Earth showing linear features along the fault trace. White arrows indicate the fault trace. See location in Fig.1b. (b) Geologic map of offset interfluves and alluvial terrace (N32º56'05.8", E103º26'38.3"). See location in Fig. 14a. (c) Topographic survey of offset terraces using RTK GPS on the south bank of Gaimalong gully, showing the displaced T2/t1 riser by 7±1 m. (d) Topographic profile across the fault scarps on the T2 terrace. See location in Fig. 14c.

Fig. 15 Determination of abandonment age of terraces (T1 and T2) and displaced landforms in the Gaimalong gully. (a) Photograph showing offset T2/T1 riser, as illustrated in Fig. 14c. Circled persons show the location of the terrace riser. (b) Fault scarp on the T2 terrace and the location of small trench. (c) OSL sample from alluvial sand lens within alluvial deposits of terrace T2. (d) OSL sample from the bottom alluvial sand in a pit on terrace T1. See sampling sites in Fig. 14b.

Fig. 16 Photograph and log of southwest wall of the trench (N32º56'05.47", E103º26'37.73"). See trench location in Figs. 14c and 15b.

Fig. 17 Relationship of the major Kunlun fault (Maqu segment) and Tazang fault. Satellite image from Google Earth.

Fig. 18 Variation of millennial slip rates from the Maqu fault segment to the Tazang fault.

Fig. 19 (a) Geodetic velocities at the eastern termination of the Kunlun fault from Gan et al. (2007). Uncertainty ellipses are plotted at 95% confidence intervals. (b) GPS velocity transect along the easternmost part of the Kunlun fault showing that the left-lateral rates on the fault decrease eastward from ~3-4 mm/yr to <1 mm/yr. See location in Fig. 19a. (c) Topographic profile across the Min Shan platform. See location in Fig. 19a. (d) GPS velocity transect across the Min Shan platform suggesting that the Min Shan platform has a crustal shortening of ~3-5 mm/yr. See location in Fig. 19a. Active faults are shown as vertical lines. HYF, Huya fault; LRBF, Longriba fault; MJF, Minjiang fault.

Fig. 20 Block diagram of the eastern termination of the Kunlun fault showing possible kinematics with adjacent active tectonics. The decrease of displacement along the eastern Kunlun fault is transformed into crustal shortening at its eastern tip. The crustal structure is from deep seismic reflection result (Wang et al., 2011).

Tables

Table 1 Radiocarbon Analytical Data[a]

Sample no.	Lab no.	GPS location	Material	$\delta^{13}C$ %	Conventional age[b] BP	Calibrated age[c] Cal BP
AX-C-2	311810	N33°49’09.78”	charcoal	-23.7	5460 ± 30	6260 ± 60
AX-C-4	306259	E103°06’08.42”	charcoal	-22.5	290 ± 30	370 ±100
AX-C-5	311811	N33°49’20.70”	organic sediment	-26.1	1980 ± 30	1930 ± 60
AX-C-7	306260	E103°05’10.88”	charcoal	-25.5	4330 ± 30	4900 ± 80
AX-C-9	306261	N33°49’12.97”	organic sediment	-26	4280 ± 30	4850 ± 60
AX-C-10	306262	E103°05’46.32”	organic sediment	-	-	-
AX-C-11	306288	N33°49’35.90” E103°04’0.20”	peat	-24.1	4180 ± 40	4270 ± 140
AX-C-12	306263	N33°49’21.10”	charcoal	-24.2	7180 ± 40	8000 ± 80
AX-C-13	306264	E103°05’10.20”	charcoal	-23.6	8190 ± 40	9150 ± 140
AX-C-14	306265	N33°49’35.90” E103°04’0.20”	organic sediment	-25.4	10840 ± 50	12720 ± 160
AX-C-15	306266	N33°49’00.54” E103°03’33.54”	organic sediment	-22.6	11390 ± 50	13260 ± 120
DB-C-2	306268	N32°56’05.47” E103°26’37.73”	charcoal	-22.7	5940 ± 40	6770 ±100
QJ-C-1	306280		charcoal	-24.8	20 ± 30	100 ± 140
QJ-C-2	311816	N33°43’34.40” E103°21’25.34”	charcoal	-24.4	2910 ± 30	3060 ± 120
QJ-C-3	306281		charcoal	-20.9	1830 ± 30	1770 ± 80
QJ-C-4	311817	N33°43’36.66”	charcoal	-23.3	2030 ± 30	1970 ± 80
QJ-C-5	306282	E103°21’26.26”	charcoal	-21.6	3980 ± 30	4460 ± 80
QJ-C-7	306284		charcoal	-23.6	1100 ± 30	1010 ± 80
QJ-C-7b	311818	N33°41’34.15” E103°08’54.14”	charcoal	-24.4	1220 ± 30	1150 ± 100
QJ-C-8	306285		charcoal	-21.9	7330 ± 40	8120 ± 120

[a]Reported ^{14}C ages used Libby’s half-life (5568 yr) and referenced to the year AD 1950. All the samples were tested by AMS at Beta Analystic.

[b]Analytical uncertainties are reported at 1σ.

[c]Calendar ages calibrated using OxCal 4.1 based on IntCal 09 curve (Reimer et al., 2009). Associated age range reported at 2σ.

Table 2 OSL age results

Lab no.	Sample no.	GPS location	K_2O %	Water content %	Dose rate Gy/ka	De Gy	Age Ka
11-OSL-284	DB-OSL-2	N33º28’21.60” E103º39’51.60”	3.84	7.91	6.13±0.52	76.50±2.85	12.48±1.10
12-OSL-74	AX-OSL-4	N33º49’00.54” E103º03’33.54”	2.66	28.79	4.56±0.11	12.11±0.67	2.66±0.26
12-OSL-86	DB-OSL-3	N32º56’7.67” E103º26’35.41”	2.85	13.46	4.89±0.44	44.06±2.44	9.01±0.88
12-OSL-87	DB-OSL-4	N33º56’7.24” E103º26’37.51”	2.66	17.88	4.76±0.42	6.56±0.30	1.17±0.11
12-OSL-88	DB-OSL-6	N32º56’05.47” E103º26’37.73”	3.15	9.70	5.62±0.49	380.71±37.86	67.70±8.64

Note: samples were analyzed in Key Laboratory of Crustal Dynamics, China Earthquake Administration.

Figure1
Click here to download high resolution image

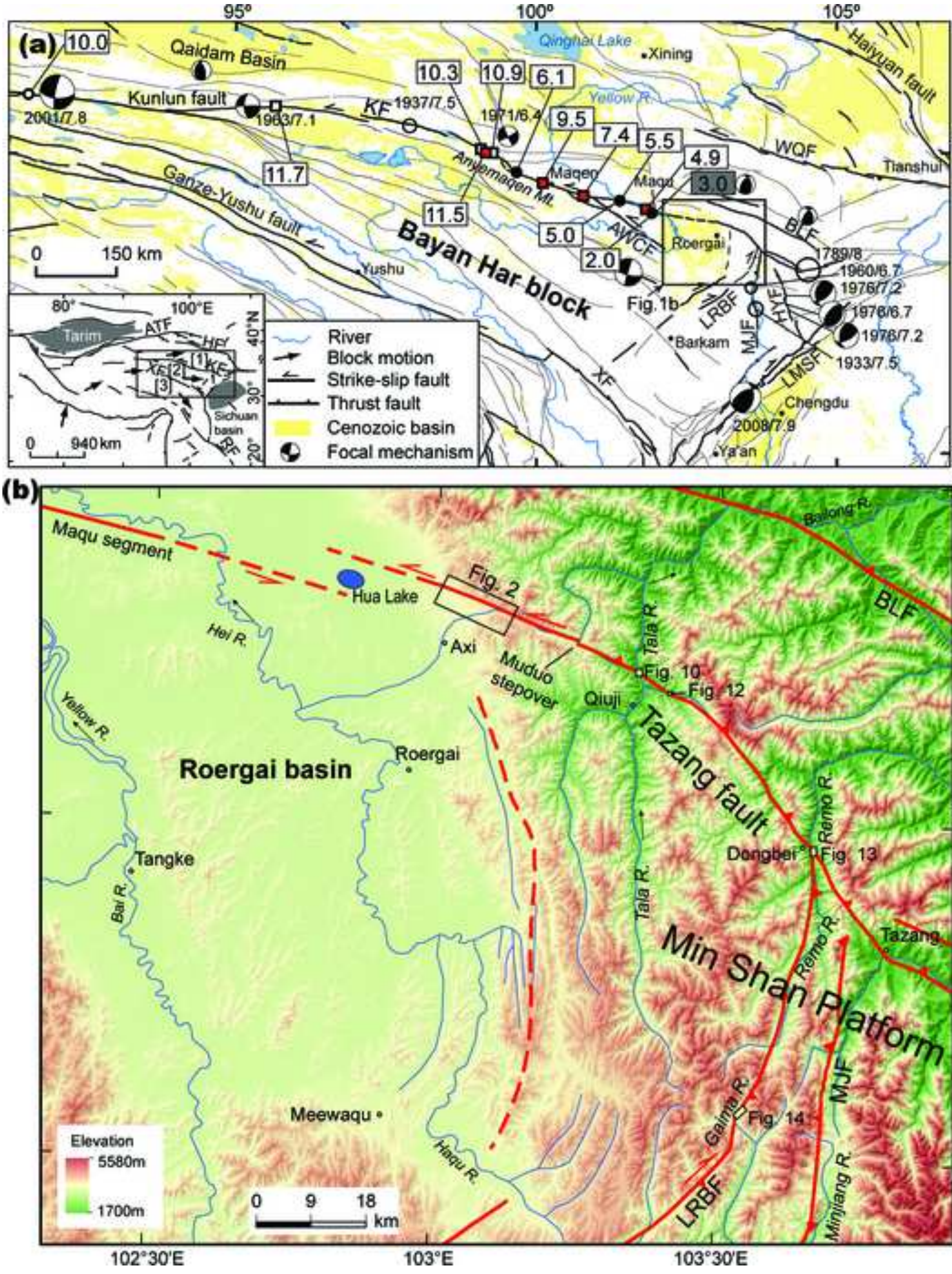

Figure2

Click here to download high resolution image

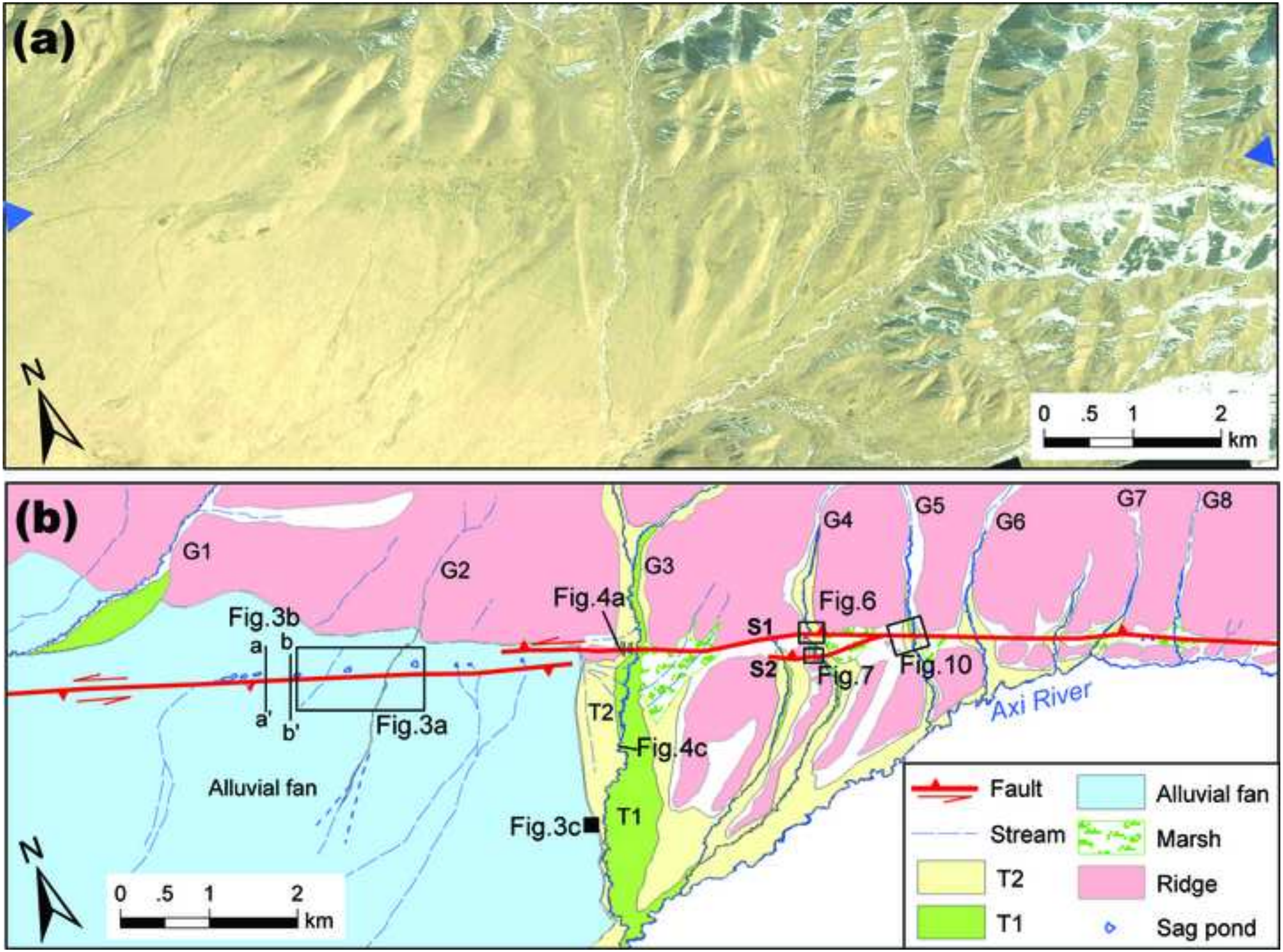

Figure3

Click here to download high resolution image

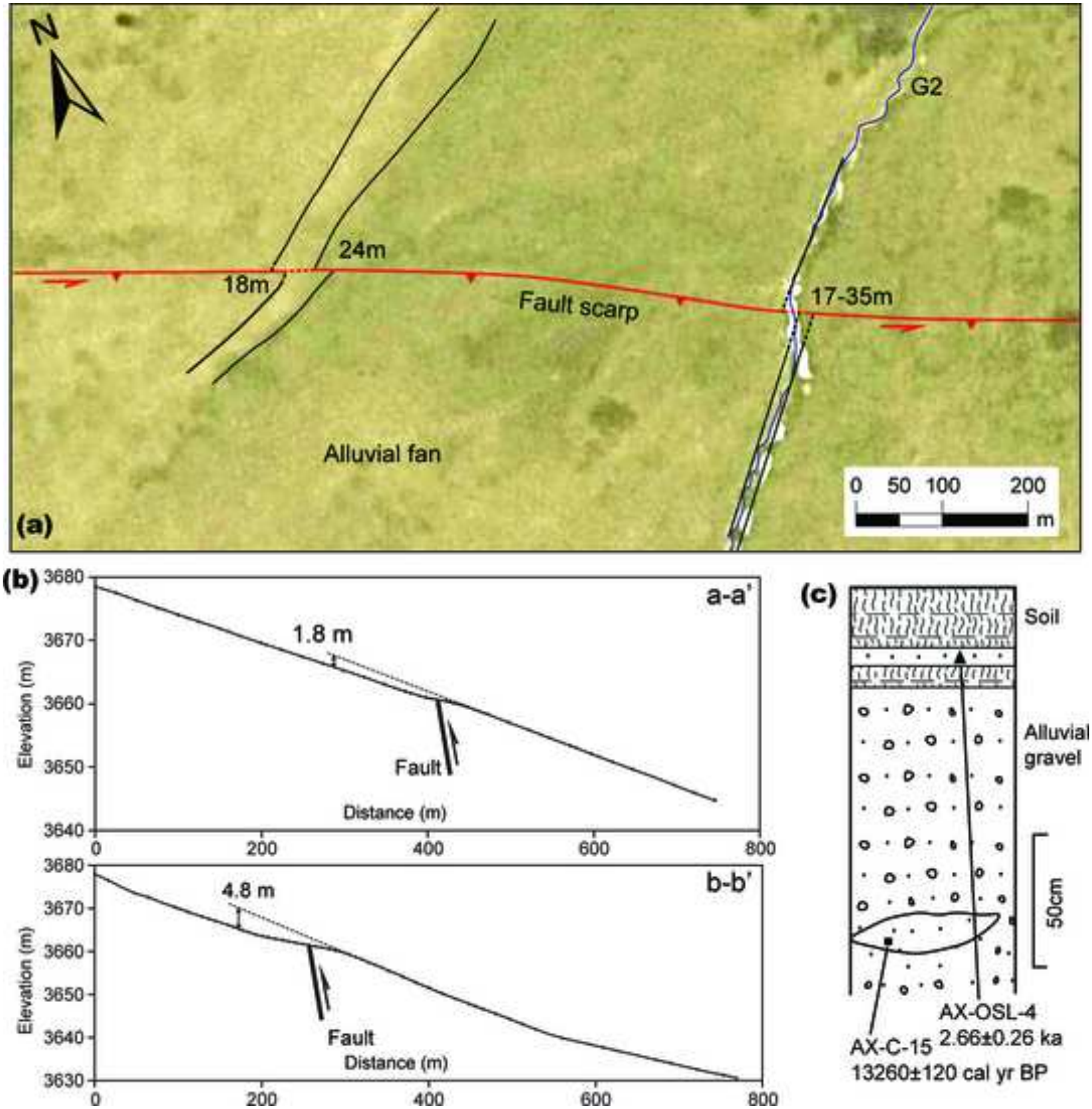

Figure4

Click here to download high resolution image

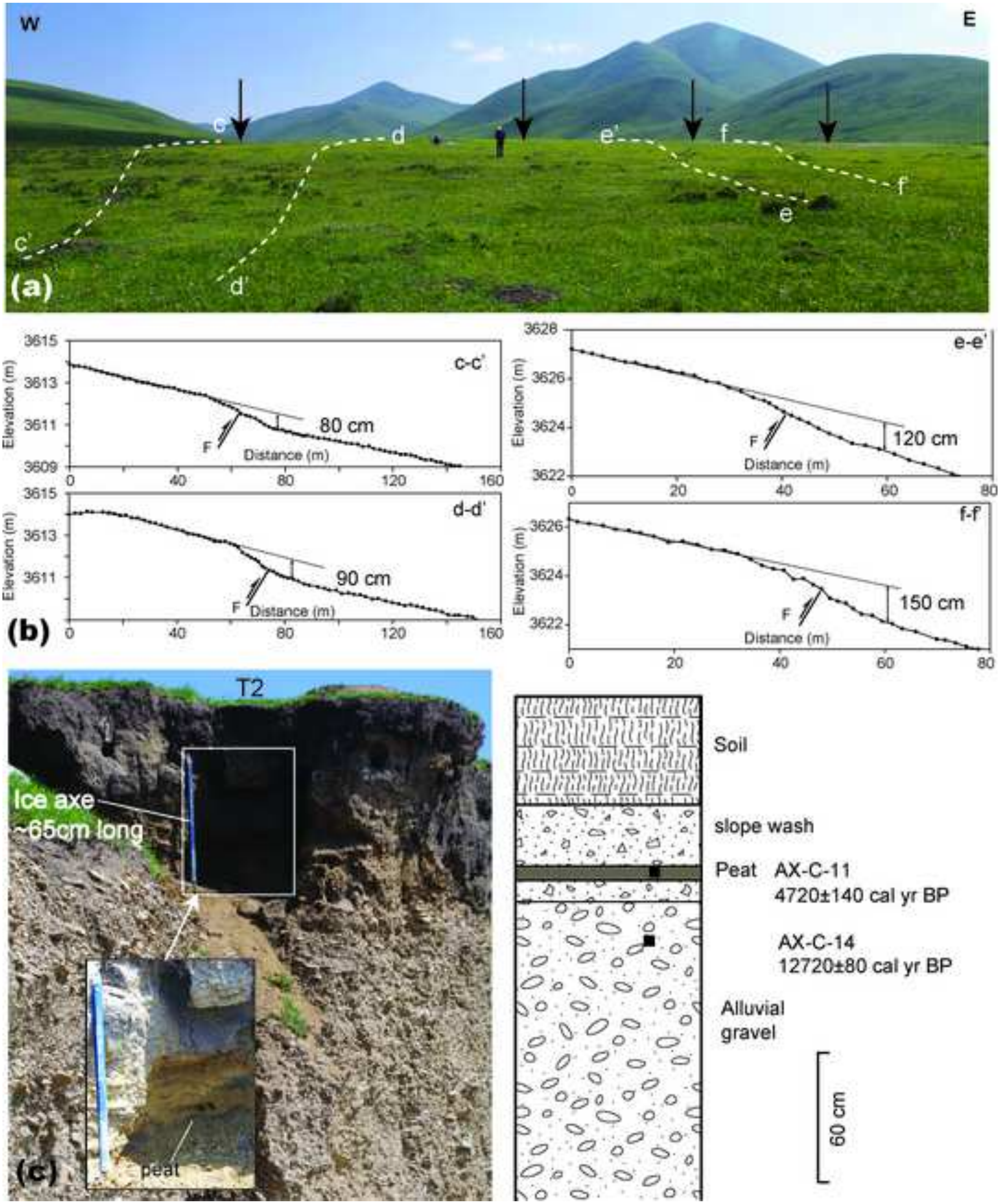

Figure5
Click here to download high resolution image

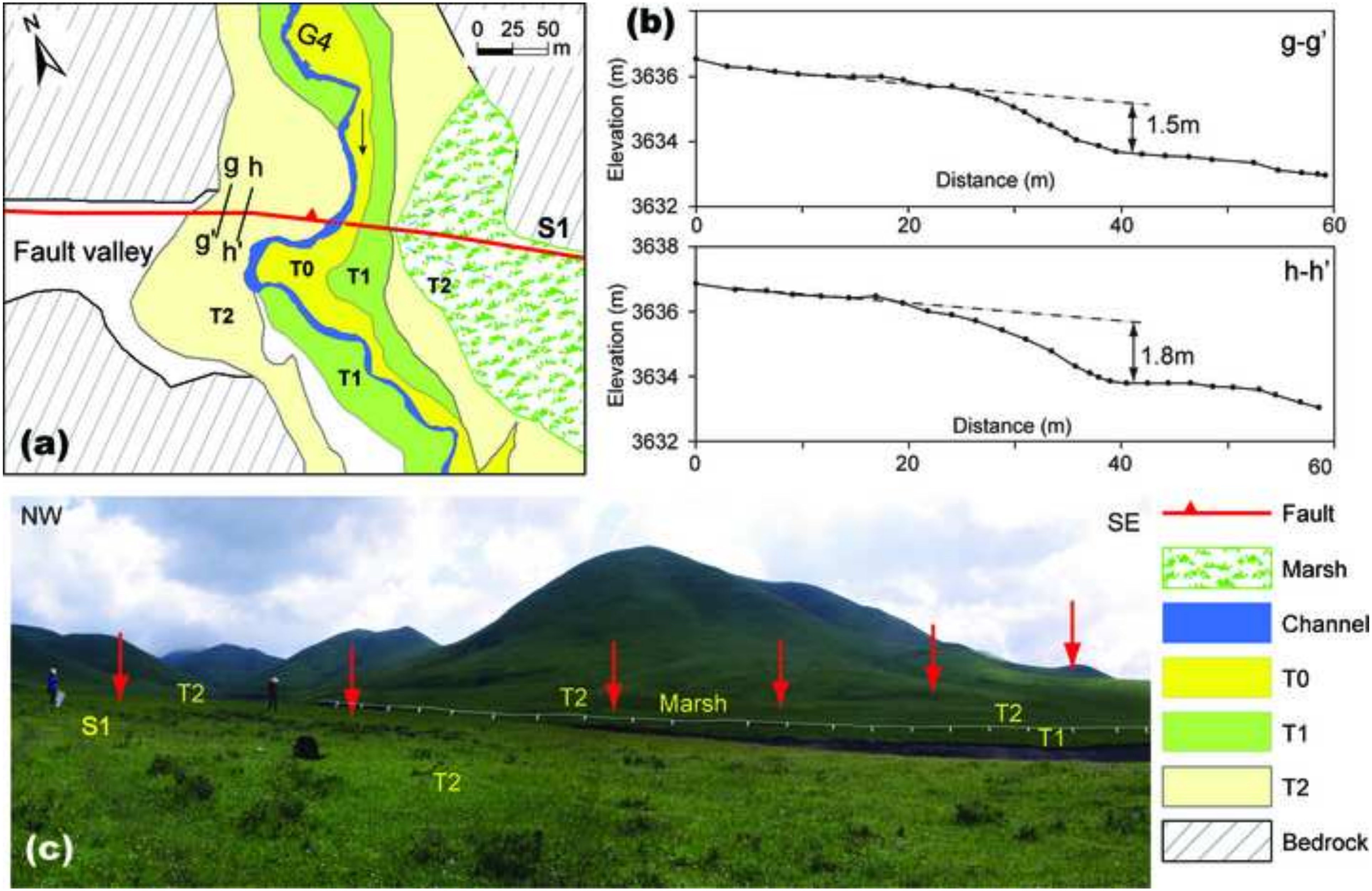

Figure6

Click here to download high resolution image

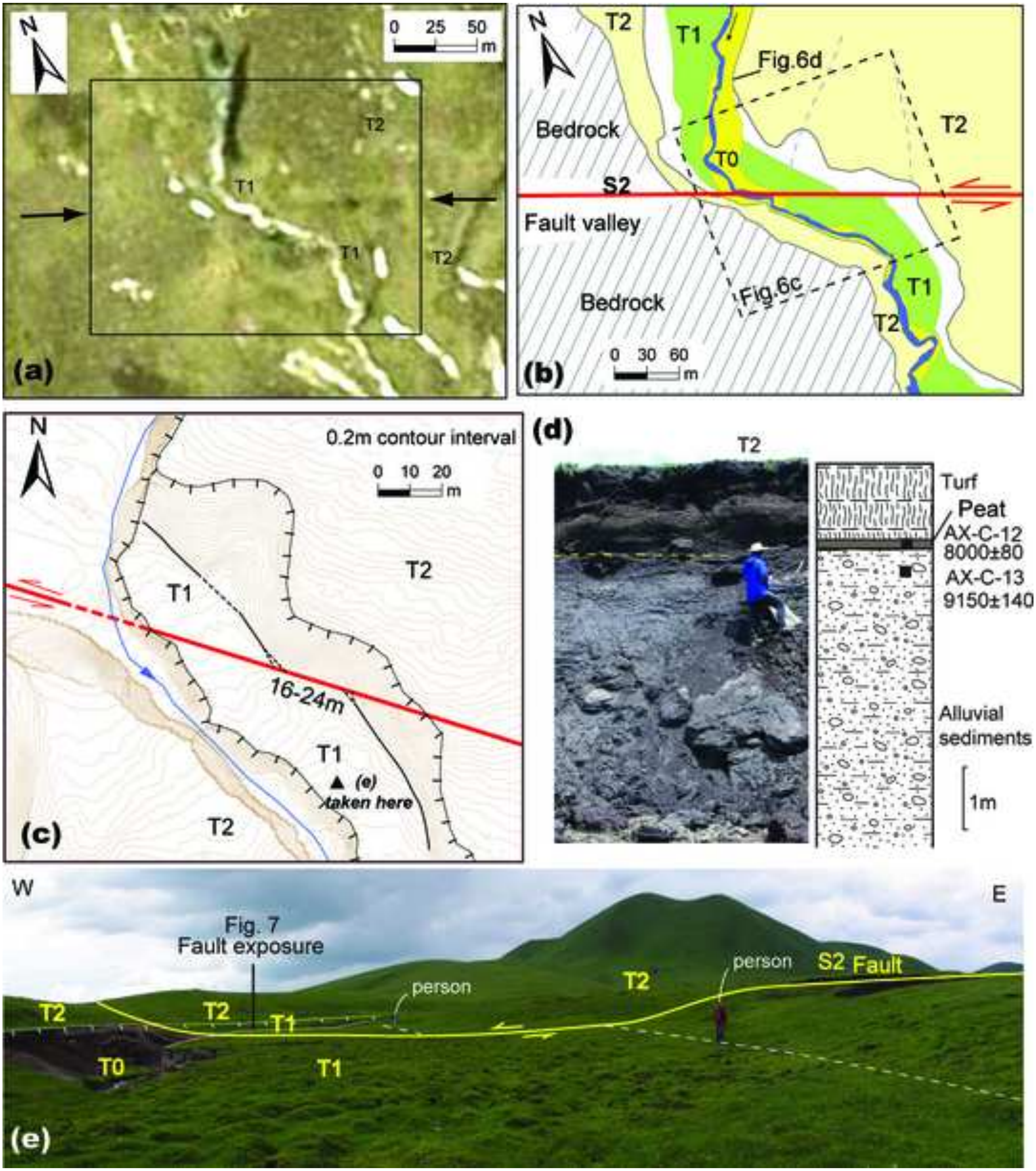

Figure7
Click here to download high resolution image

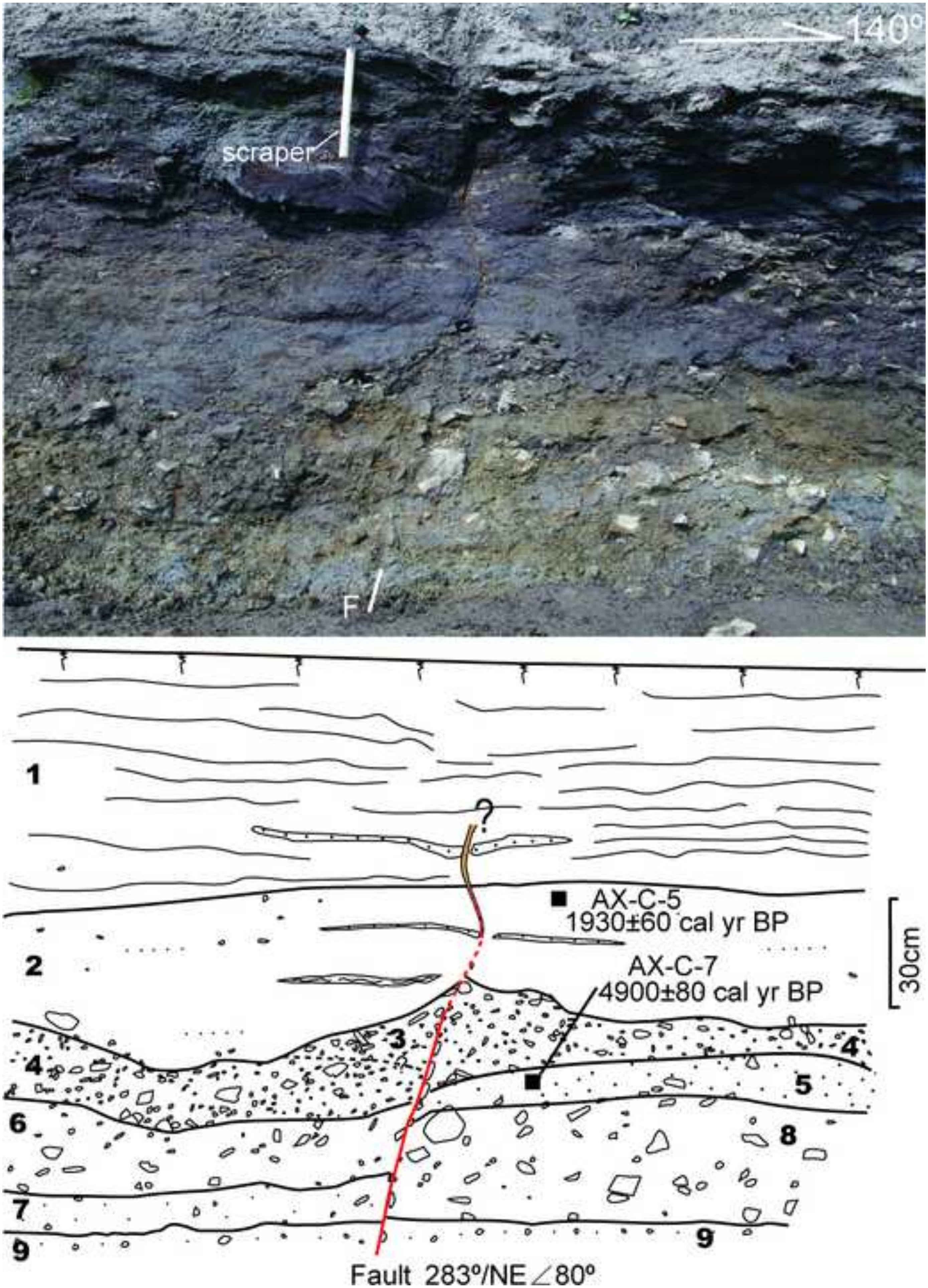

Figure8

Click here to download high resolution image

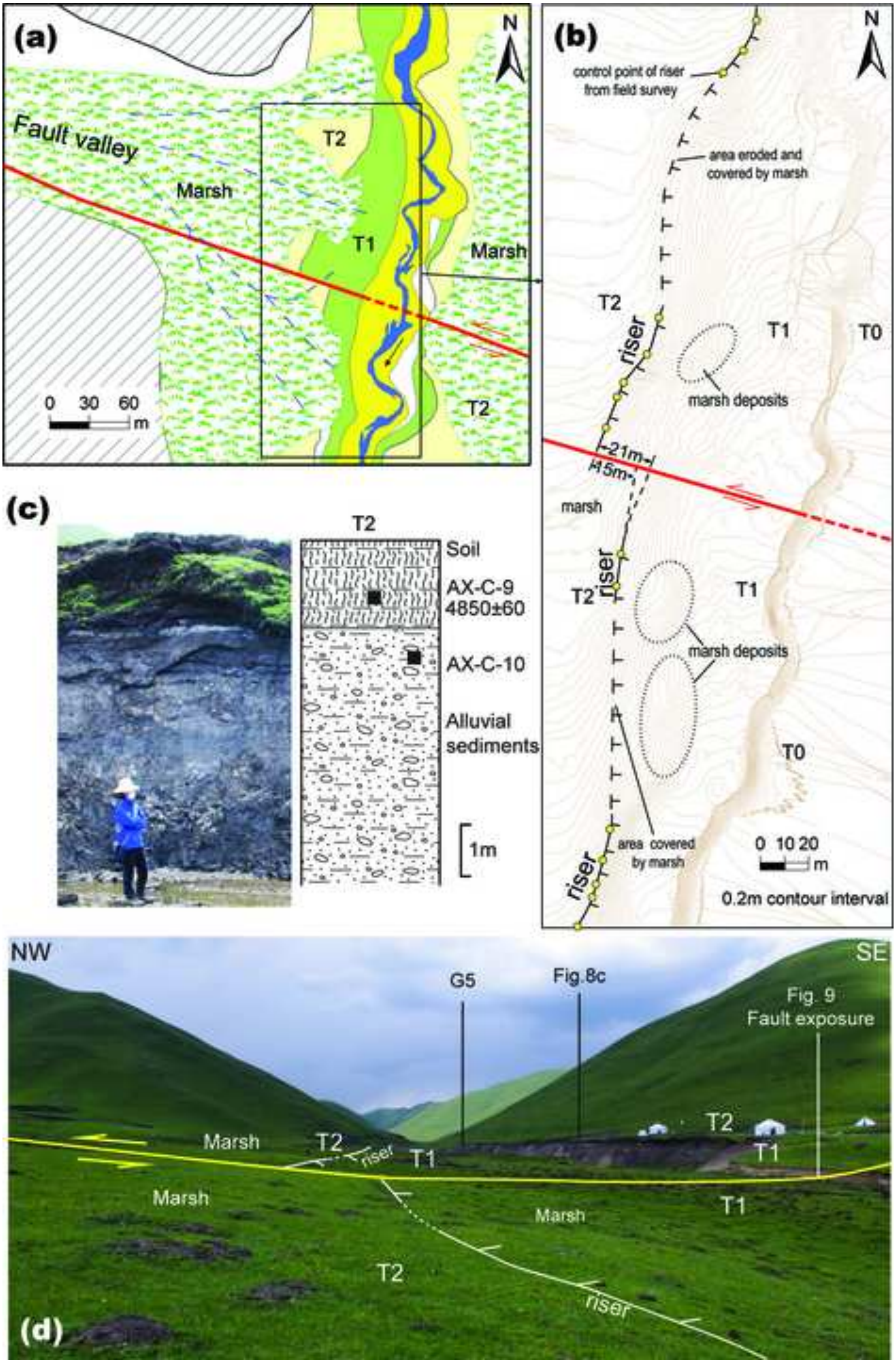

Figure9

Click here to download high resolution image

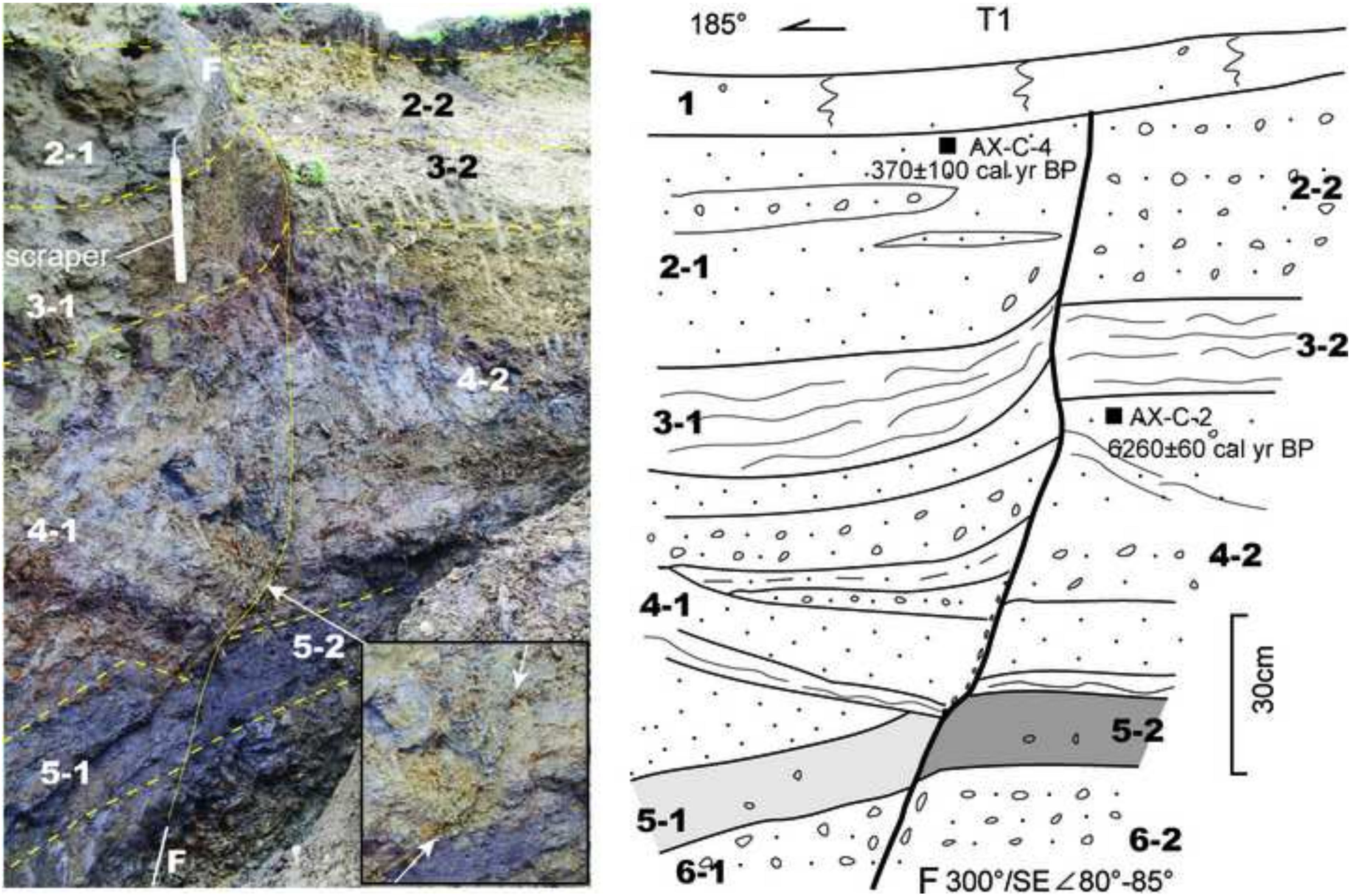

Figure10
Click here to download high resolution image

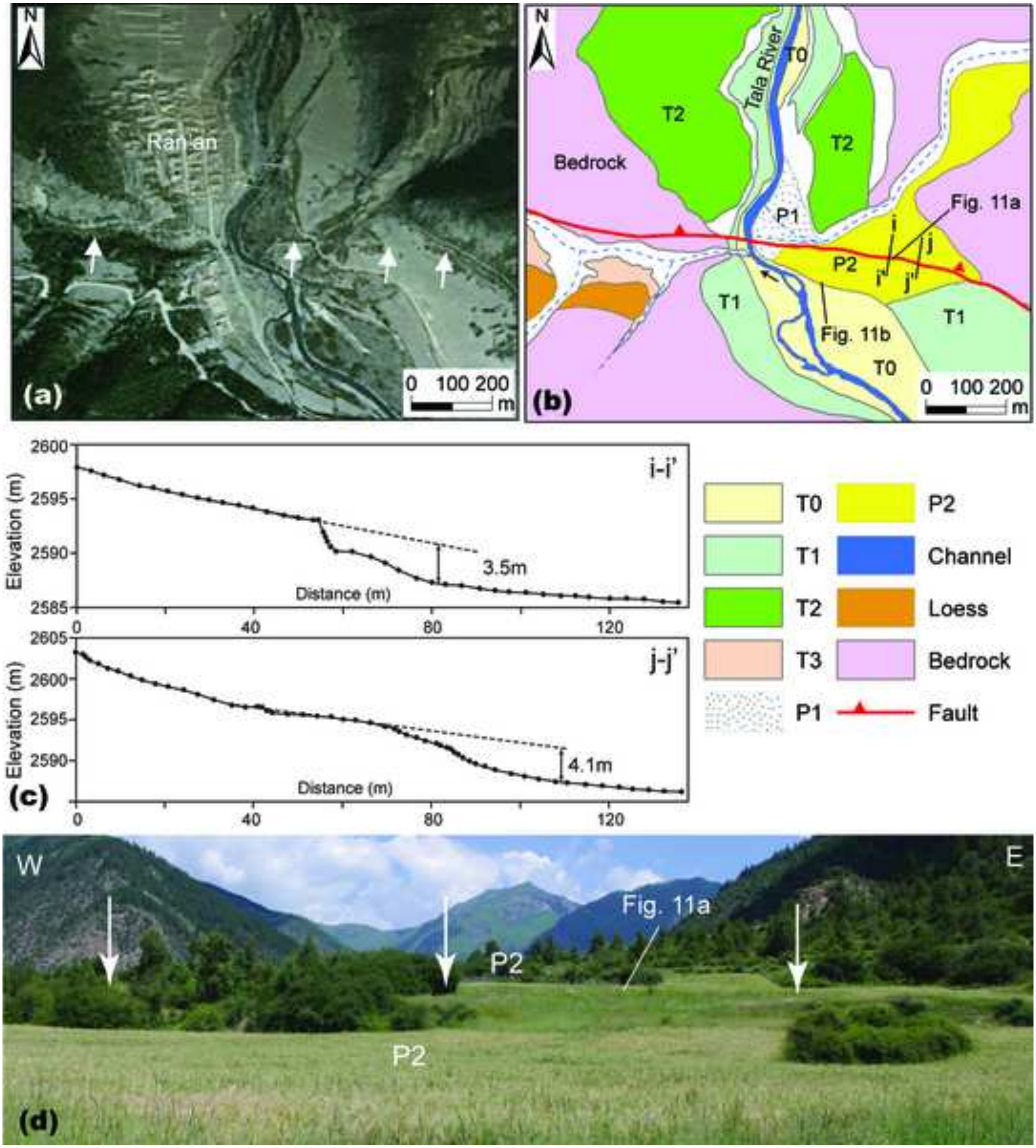

Figure11
Click here to download high resolution image

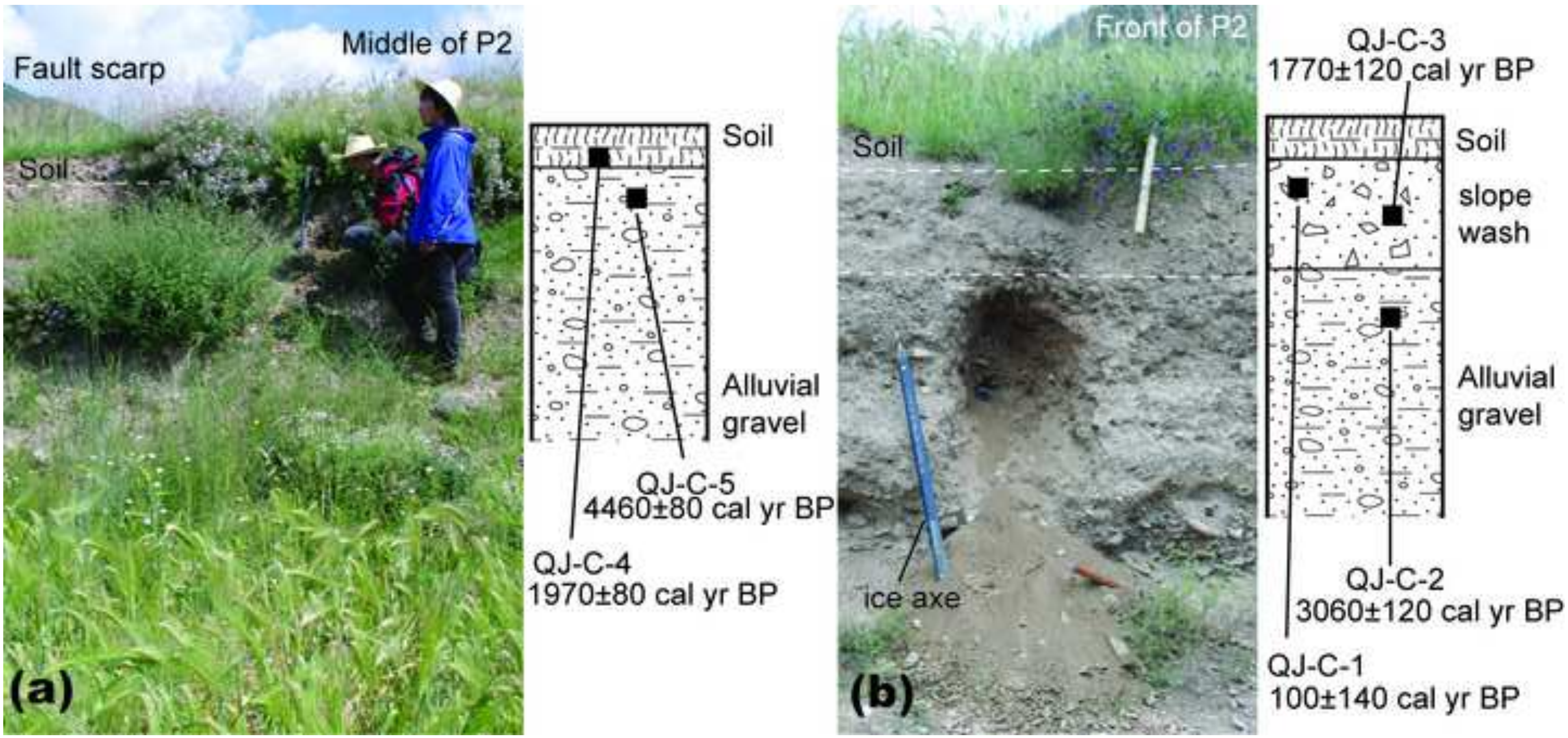

Figure12
Click here to download high resolution image

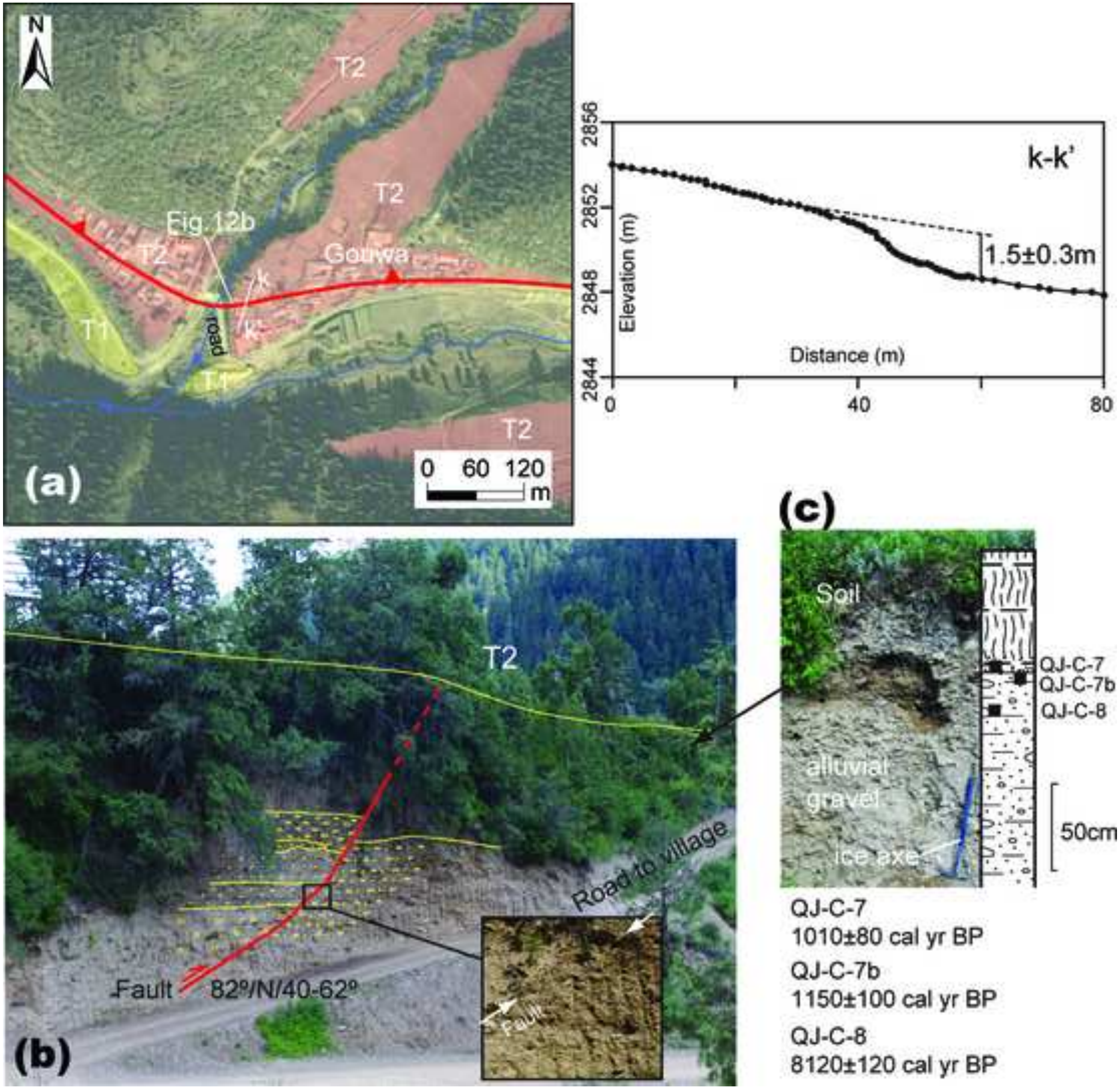

Figure13

Click here to download high resolution image

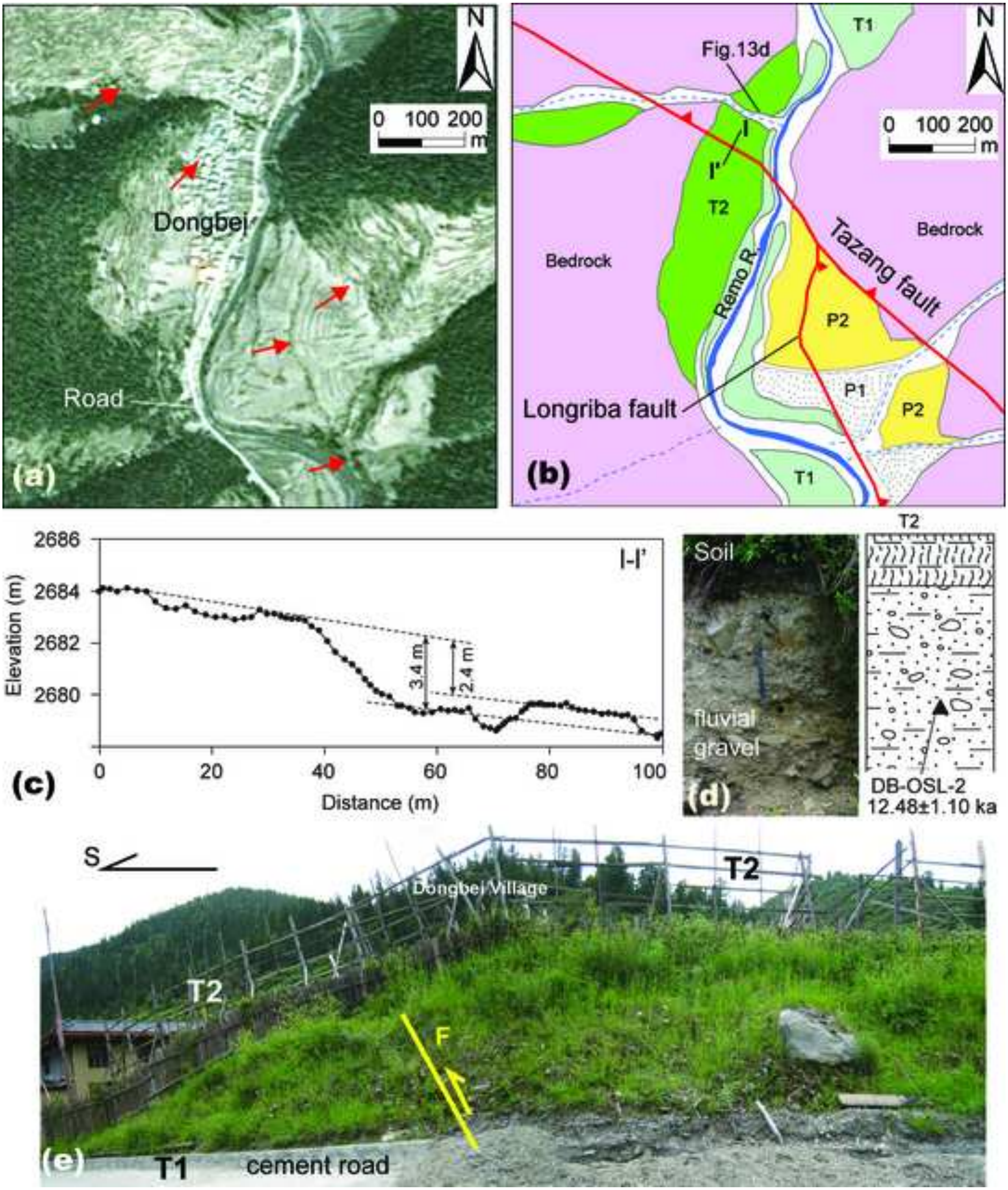

Figure14
Click here to download high resolution image

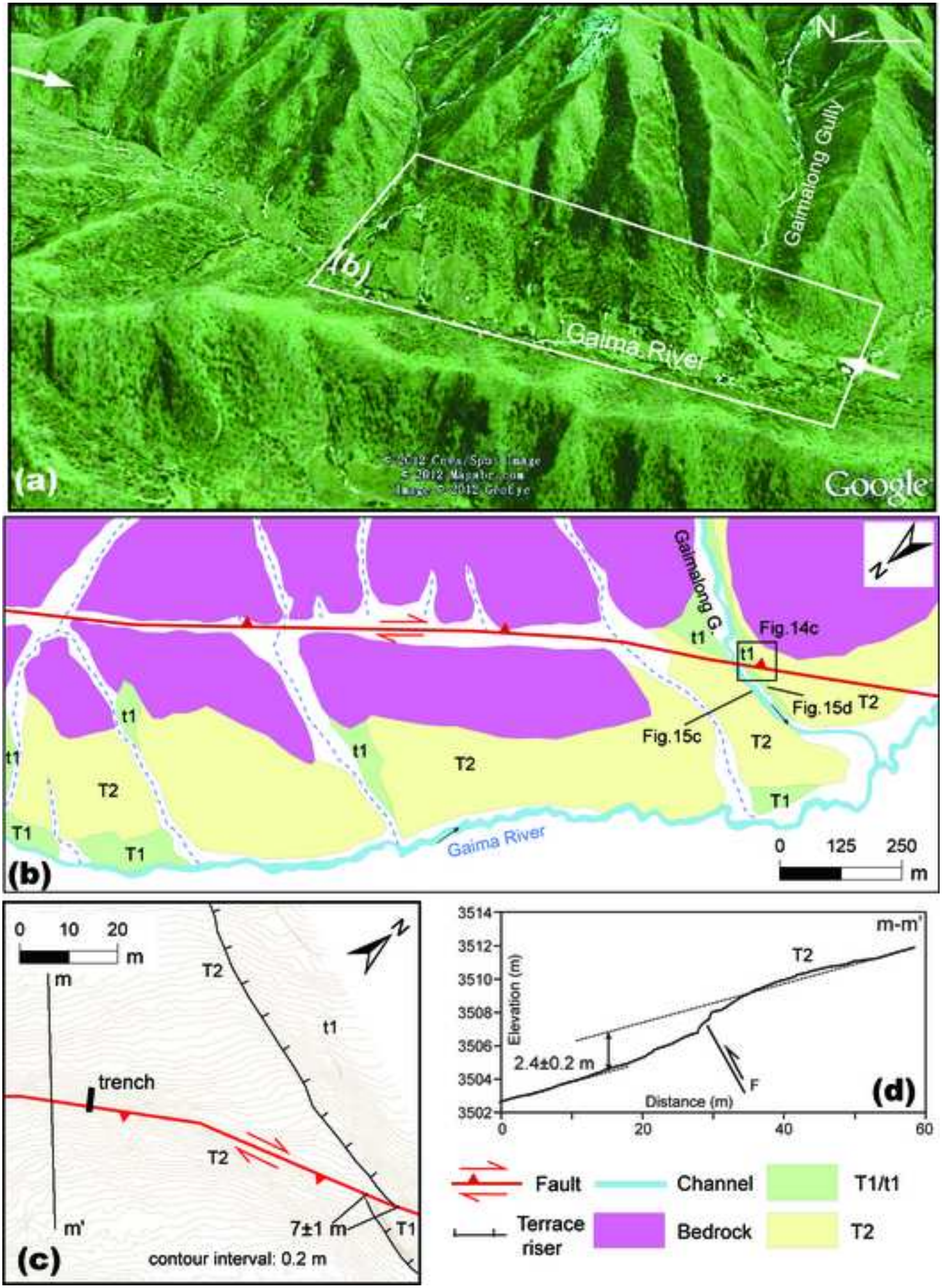

Figure15
Click here to download high resolution image

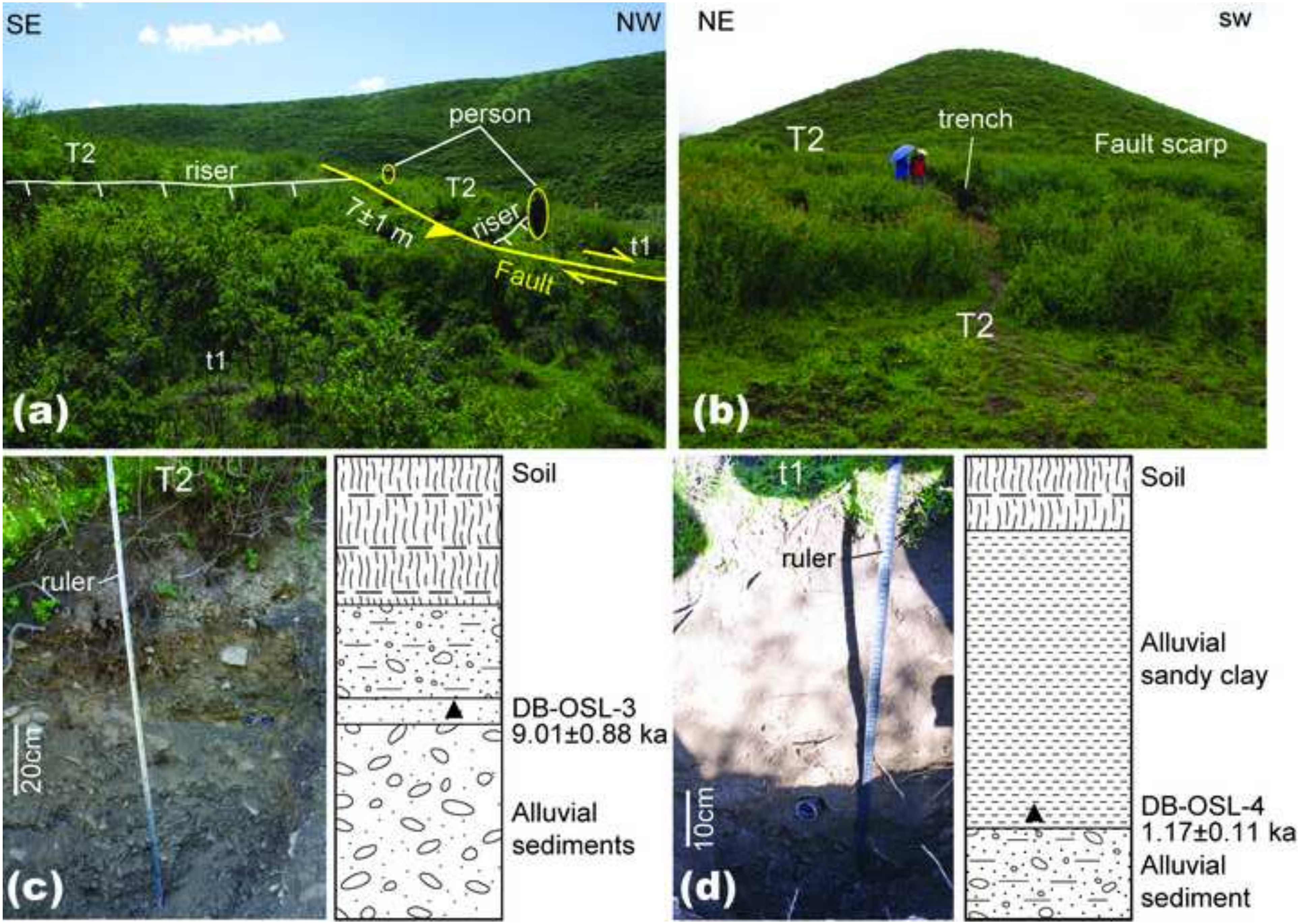

Figure16

Click here to download high resolution image

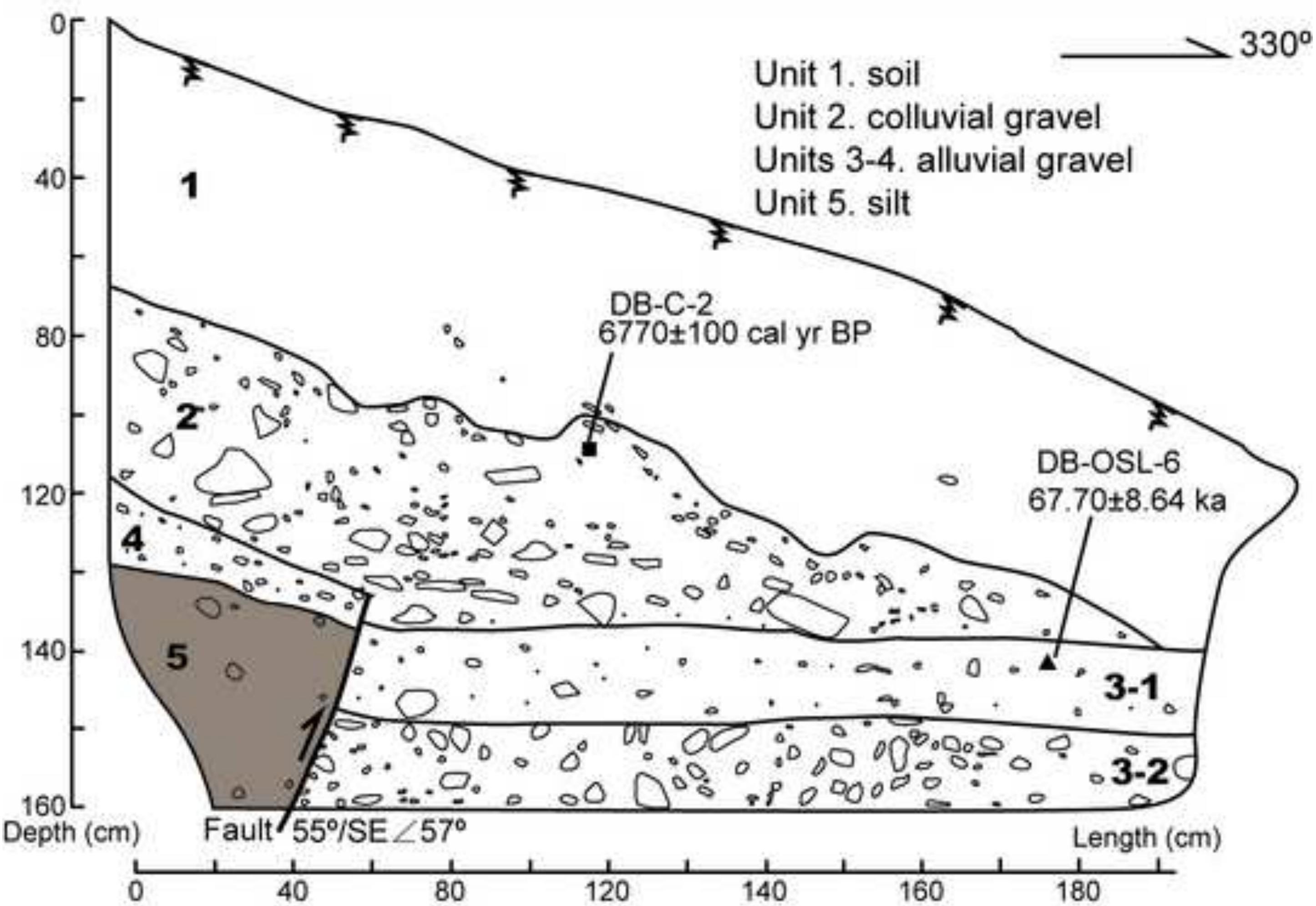

Figure17
Click here to download high resolution image

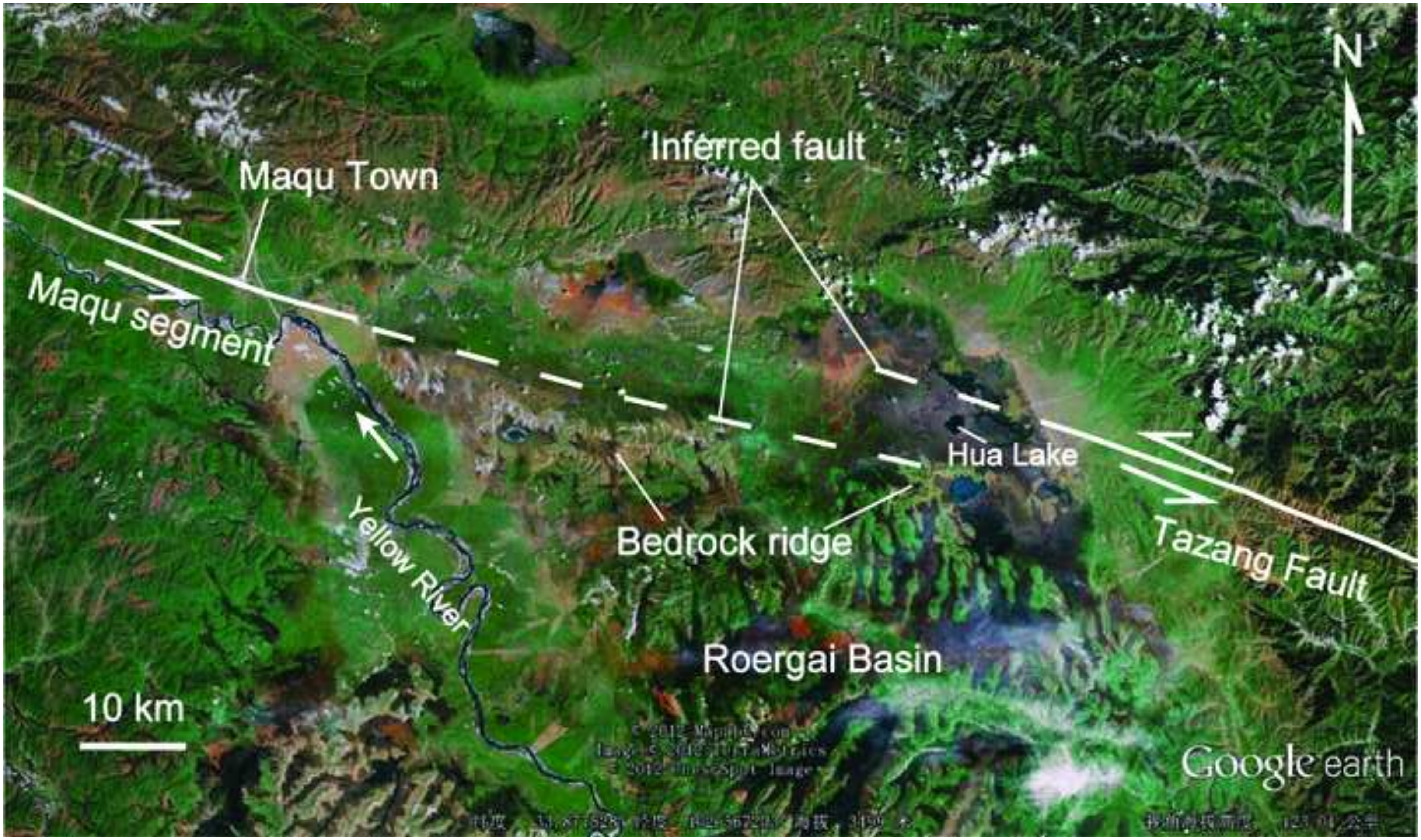

Figure18
Click here to download high resolution image

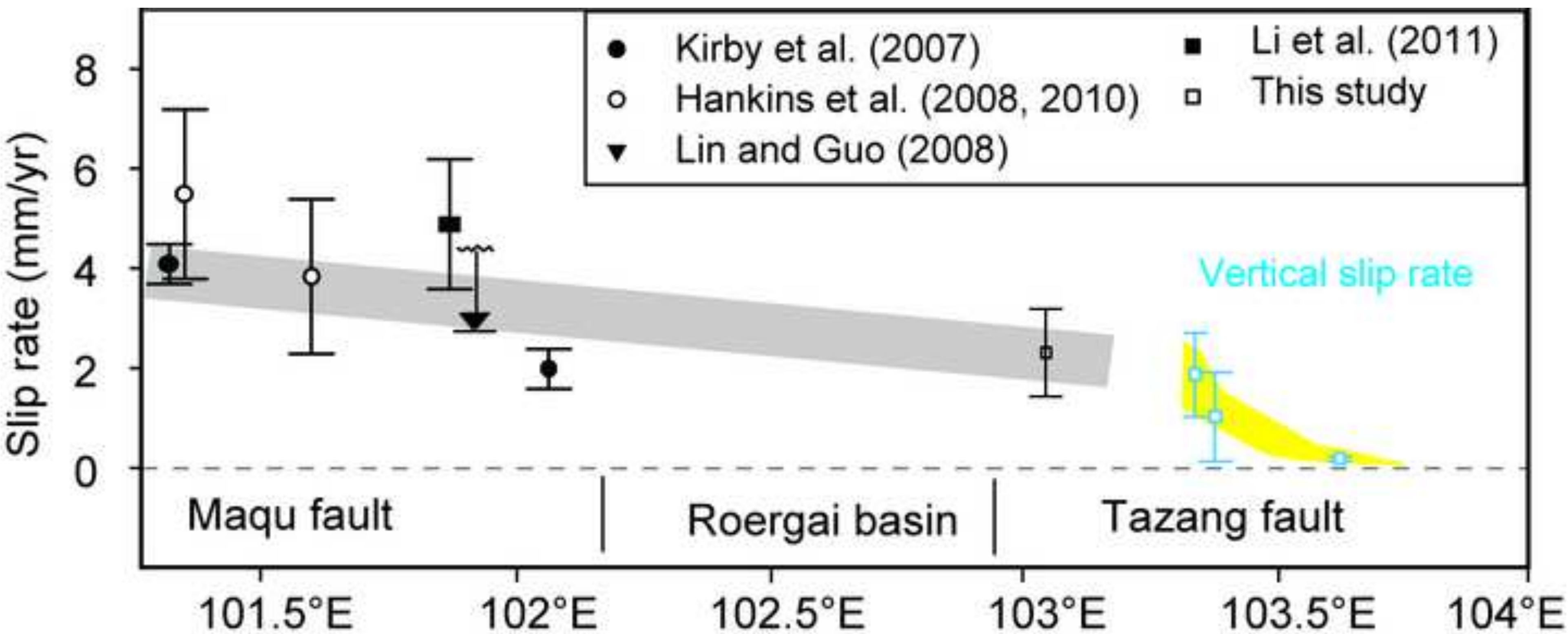

Figure19
Click here to download high resolution image

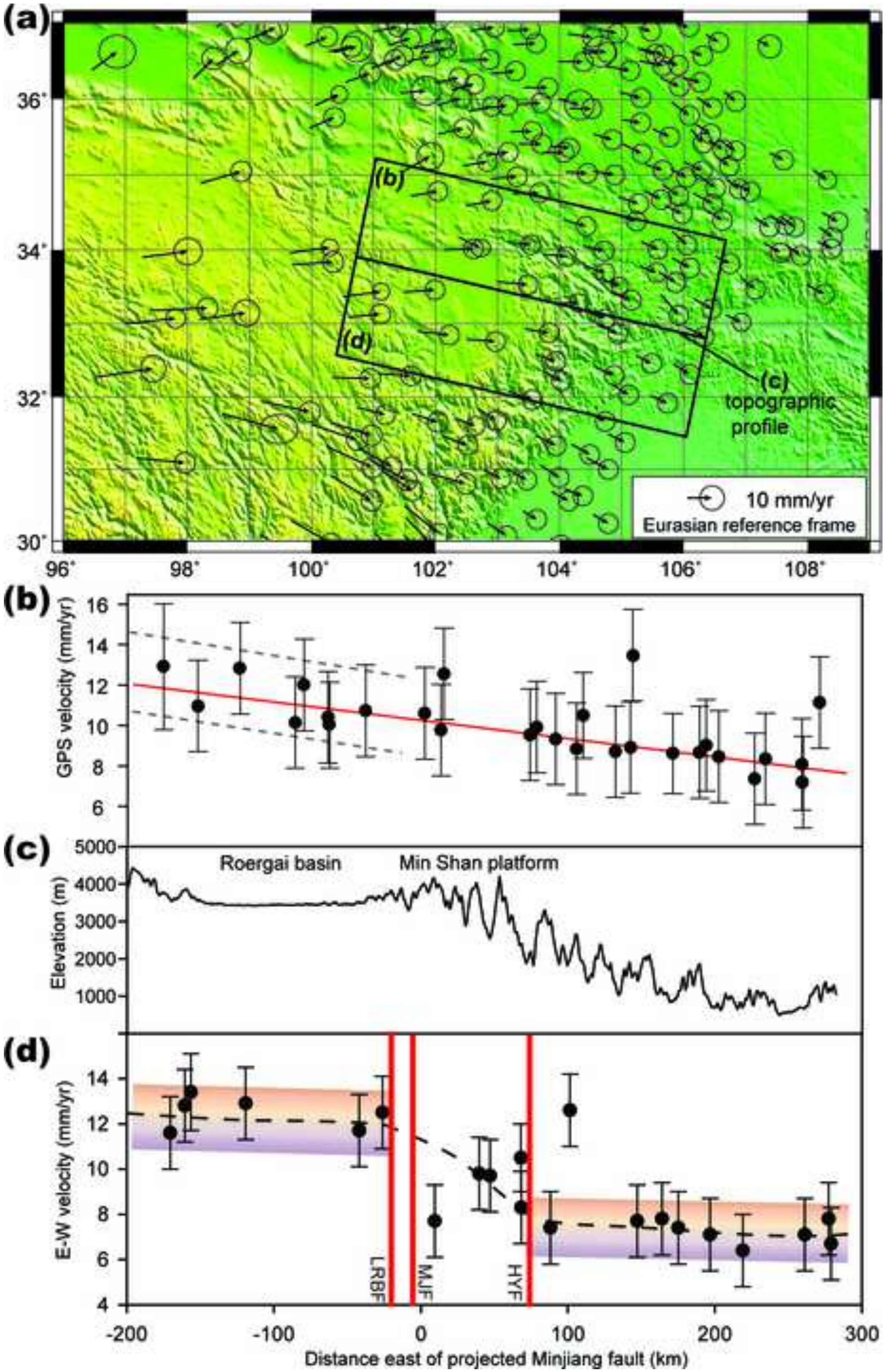

Figure20

Click here to download high resolution image